國立交通大學

電子工程學系 電子研究所碩士班

碩 士 論 文

精確且高效率之
蕭基位障萃取程序

An Accurate and Efficient Procedure for Schottky Barrier Height Extraction

研究生：傅子瑜

指導教授：崔秉鉞 教授

中華民國一 O 一年十二月

精確且高效率之蕭基位障萃取程序

An Accurate and Efficient Procedure for Schottky Barrier Height Extraction

研究生：傅子瑜　　Student : Tz-Yu Fu

指導教授：崔秉鉞　　Advisor : Bing-Yue Tsui

國立交通大學

電子工程學系 電子研究所

碩士論文

A thesis

Submitted to Department of Electronics Engineering and Institute of Electronics

College of Electrical Engineering and Computer Engineering

National Chiao Tung University

In Partial Fulfillment of the Requirement

for the Degree of

Master of Science

in

Electronics Engineering

2012

Hsinchu, Taiwan, Republic of China

中華民國一Ｏ一年十二月

精確且高效率之蕭基位障萃取程序

研究生：傅子瑜　　指導教授：崔秉鉞

國立交通大學

電子工程學系　電子研究所碩士班

摘要

隨著半導體製程微縮，半導體元件的接觸電阻也因為面積縮小而增大，而晶片迴路的總驅動電流也因此被降低。為了繼續微縮元件，如何有效降低接觸電阻變成是一個重要議題。而接觸電阻與蕭基位障、基板濃度等因素息息相關，因此可藉由調整此兩種參數去降低接觸電阻。許多研究指出經由特定製程可有效降低蕭基位障，例如：離子佈植、熱退火處理，並給出等效的蕭基位障值。然而這些蕭基位障都是藉由熱游離模型萃取而得，而只採用熱游離模型的傳導機制對於萃取蕭基位障並不足夠。經過特定製程之元件，其半導體表面電場可能已被大幅提升，電流傳導機制也可能不再是熱游離模型主導。因應高電場效應，場發射模型應被考慮在傳導機制中。藉由萃取正確的蕭基位障，經由特定製程所導致之實際影響才能被正確討論及應用。

本研究建立一完整考慮熱游離、場發射、鏡像電荷導致位障降低及寄生電阻等機制的蕭基位障擷取程序。經以技術電腦輔助設計軟體模擬，驗證此程序之正確性。不同位障高度、不同基板濃度以及非均勻摻雜之基板也在模擬作業中被完整討論。更進一步地研究各種材料之基板所形成的蕭基接面，以及不同離子佈植條件之影響，最後再探討本程序對於萃取極低蕭基位障之可行性。

在模擬作業中，模擬工具與實際之鏡像電荷導致位障降低機制之差異已被完整討論。由於模擬工具中的鏡像電荷導致位帳降低機制模型過度簡化，導致模擬結果不能完全符合實際之蕭基接面。在不同基板濃度之模擬中，討論了電流密度隨逆偏電壓之變化。由於高濃度基板造成更嚴重的鏡像電荷導致位帳降低之影響，

對數軸中電流密度對電壓之斜率會隨著濃度提升。在非均勻摻雜之基板模擬中，討論了表面濃度提升之影響。表面濃度提升並不會降低蕭基位障，而只是造成更嚴重的鏡像電荷導致位障降低之影響。

在實驗中驗證了此萃取程序對於不同基板材料，例如：碳化矽、鍺、矽，之可行性。另外，碳離子佈植對矽化鎳/矽接觸面之蕭基位障高度的影響也在此被討論。從程序中萃取之蕭基位障及載子濃度得知，碳離子佈植對蕭基位障並無作用，僅僅只是提升等效載子濃度。再來藉由矽化鉑/矽接觸面之蕭基接面探討此程序對於極低蕭基位障萃取之可行性。蕭基位障隨溫度變化之現象在低溫測量被觀測到，而其可能是由於半導體表面能階改變導致費米能階鎖定位置不同。最後研究了氟化硼離子佈植對蕭基接面之影響。跟模擬結果作比較後，我們相信硼離子會加強鏡像電荷導致位障降低之效果，而氟離子會有修補表面能階之功能。

本研究提出了一項快速且準確的蕭基位障擷取程序。擷取過程僅需數十秒，且量測得到的數據不需要額外的人工處理。因此，特定製程對蕭基接面之影響可以被正確地探討及應用。

An Accurate and Efficient Procedure for Schottky Barrier Height Extraction

Student: Tz-Yu Fu Advisor: Bing-Yue Tsui

Department of Electronics Engineering

Institute of Electronics

National Chiao Tung University

Abstract

As the scaling of the semiconductor fabrication process, the contact resistance in semiconductor devices becomes larger due to the smaller contact area, and the total driving current is degraded. How to reduce the contact resistance is an urgent issue for the continued scaling. Contact resistance is highly dependent on the Schottky barrier height (SBH) and the substrate doping concentration, so they can be lowered by adjusting these two parameters. Several studies have been proposed that the SBH can be lowered by some specific fabrication processes, for example ion implantations and thermal annealing, and those literatures reported the effective SBHs. However, these SBHs are extracted by the thermionic emission (TE) model, and it is not adequate for extracting the actual SBH. For the devices after specific fabrication process, the electric field near the semiconductor surface may be intensively increased, and the conducting mechanism may be no longer dominated by the TE model. For the high electrical field, the field emission (FE) model should be considered into the conducting mechanism. Without extracting the actual SBH, the effect of the specific fabrication process cannot be correctly discussed and applied.

In this thesis, we setup a procedure to extract the SBH considering thermionic emission, field emission, image-force barrier lowering (IFBL) model and parasitic resistance thoroughly. The validity of the proposed procedure is verified and confirmed by technology CAD tool. Different SBHs and different substrate doping profiles have been discussed in the simulation work. Furthermore, the Schottky junctions on different semiconductor materials and the effects of ion implantations are studied, and the validity of extracting the exact low SBHs is discussed at last.

In the simulation work, the difference of the IFBL models between the real case and the simulating tool is explored. The IFBL model in the simulation tool is too simple to fit the real Schottky junction. In the simulation of different substrate doping concentrations, the current-voltage characteristics at reverse bias are discussed. The slope in the log(J)-V raises as the concentration increases due to the severe IFBL effect. In the simulation of non-uniformly doped profiles, it is observed that the increasing of the surface doping concentration does not lower the actual SBH but induce severe IFBL effect.

In the experiment, the validity of extracting the SBHs on various semiconductor materials including silicon carbide, germanium, and silicon, by the proposed procedure is verified. Furthermore, the effect of carbon ion implantation on the SBH of NiSi/Si contact is discussed. The extracted SBH and doping concentration show that the carbon ion implantation does not change the SBH but simply increases the effective carrier concentration. The validity of the exact low barrier height extraction is verified through the case of PtSi/Si Schottky junction. The temperature dependence of the SBH is observed at low temperature, and it is believed that the make-up of the surface states is changed and results in Fermi-level pinning at different energy levels. Finally, the effect of BF_2^+ ion implantation on the Schottky junction is discussed. In comparison with the simulation results, it is believed that the increasing boron ions

enhance the IFBL effect and the fluorine ions have the ability to repair the surface states.

This thesis proposes an efficiency and accurate procedure for the SBH extraction. It only takes about tens of seconds, and it is not necessary to cope with the measured data artificially. The effect of the specific fabrication process on the Schottky junctions can be correctly discussed and applied.

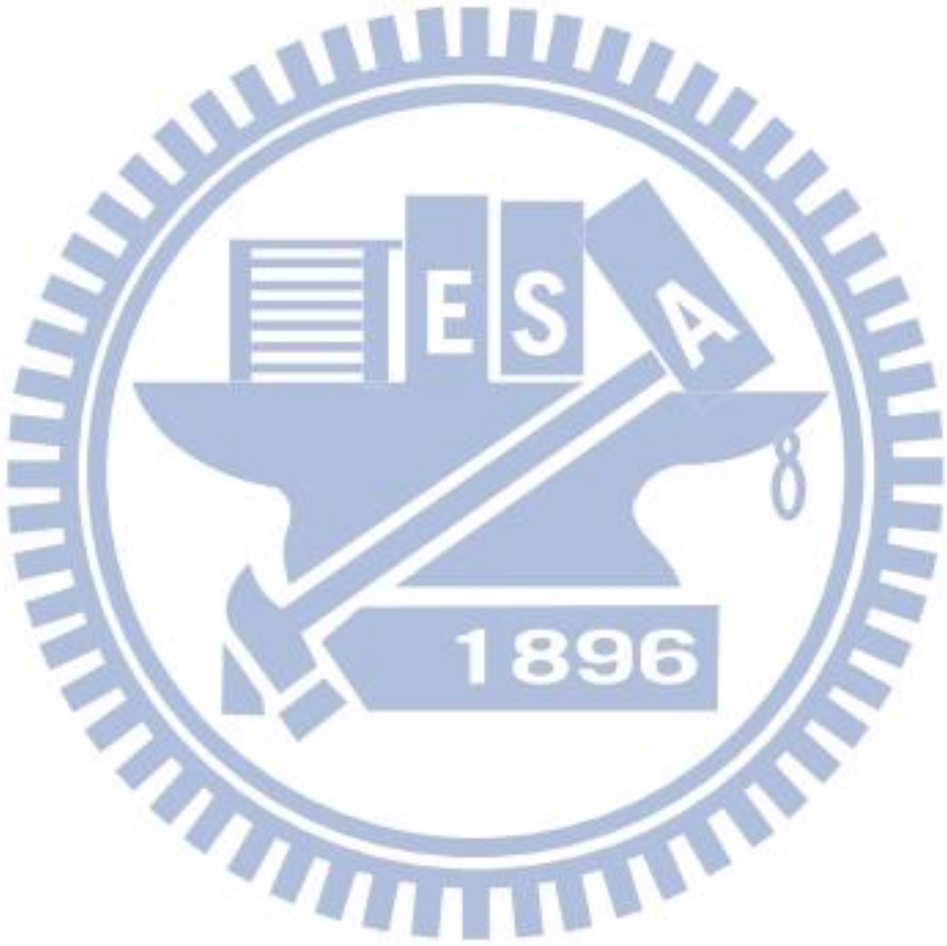

致謝

此篇論文承蒙許多人的幫助才得以完成，過程中遇到許多挫折與困難也讓我成長、學習許多。謹以此文來感激這兩年內幫助我的人們。

首先，感謝我的指導教授 崔秉鉞老師。從大學做專題時期就開始指導我如何正確地做研究、有效率地分析數據與討論，在老師的悉心指導下讓我成長許多，不只是做研究，也學習到如何能更圓融地去待人處事。

感謝實驗室的大家，振銘、嶸健、元宏、培宇學長無論是在訓練機台、實驗討論都給予我相當大的幫助。另外感謝高銘鴻同學，從大學做專題時就是一直陪我討論的夥伴，研究上很多不了解的東西都是在跟他的討論過程中慢慢摸熟。此外，定業學長也在我車禍期間幫我準備上課筆記讓我修課順利完成。同居同學克勤、茂元、孫銘鴻也在我腳行動不便時，在實驗上幫助了我許多。另外感謝單哥王培宇，在兩年枯燥乏味的實驗生活中，他的幽默風趣帶給實驗室許多歡笑，崇德、哲儒、雪君、翰奇、泰源與國丞也讓我的實驗生活添增許多樂趣。

再來感謝我的女朋友炫滋，總是適時地幫我分擔壓力與鼓勵，讓我能有動力再往下一步邁進。最後感謝我的父母，在車禍期間的照顧與鼓勵讓我不意志消沉，更讓我能無後顧之憂地進行研究，謝謝你們。

Contents

Abstract (Chinese) i

Abstract (English) iii

Acknowledgements vi

List of Tables ix

List of Figures xi

Chapter 1 Introduction……1

1-1 Fundamental Properties of Schottky Barrier……1

1-1.1 Schottky barrier……1

1-1.2 Fermi-level Pinning……..3

1-1.3 Barrier Lowering……..3

1-2 Potential Application of Low Schottky Barrier……..4

1-3 Conducting Mechanism in the Schottky Barrier……5

1-4 Traditional Extraction Method of the Schottky Barrier……...6

1-4.1 Current-Voltage Method……..6

1-4.2 Capacitance-Voltage Method……..7

1-4.3 Photoelectric Method……..8

1-4.4 Activation Energy Method……..8

1-5 Motivation……9

1-6 Organization……..10

Chapter 2 Extraction Model and Experiments……17

2-1 Extraction Model……..17

2-2 Simulation Settings……..20

2-3 Experiment Settings……21

2-4 Device Fabrication……...22

2-5 Low temperature measurement……..24

Chapter 3 Simulation Results and Discussion…….35

3-1 Schottky Barriers with Constant Doping Profile……..35

3-1.1 Difference between Simulation and Extraction Model……36

3-1.2 The Temperature Limits of Extraction Models……37

3-1.3 Effects of the Doping Concentrations……..38

3-2 Schottky Barriers with Gaussian Doped Profile……...39

3-2.1 Effects of the Peak Concentration……39

3-2.2 Effects of the Junction Depth……...41

3-3 Summary……..42

Chapter 4 Experiment Results and Discussion……53

4-1 Medium and High Height Extractions……53

4-1.1 Metal/n-SiC Schottky Junctions……..53

4-1.2 Effect of Carbon Ion Implantation……...54

4-2 Low Barrier Height Extractions……...56

4-2 .1 Study of NiGe/n-Ge Schottky Junction……56

4-2 .2 PtSi/ and NiSi/p-Si Schottky Junction……57

4-2 .3 Effect of BF2+ Ion Implantation……..58

4-3 Temperature Dependence……59

4-4 Summary……..60

Chapter 5 Conclusions and Future Works……..73

5-1 Conclusions……..73

5-2 Future Works……75

References……77

Author's Biography……....85

List of Tables

Chapter 3

Table 3-1 Traditional TE extraction result of barrier height set to 0.5 eV with constant doping profile……..44

Table 3-2 TFE extraction result of barrier height set to 0.5 eV with constant doping profile……...44

Table 3-3 Traditional TE extraction result of barrier height set to 0.3 eV with constant doping profile……..44

Table 3-4 TFE extraction result of barrier height set to 0.3 eV with constant doping profile……...……...44

Table 3-5 Traditional TE extraction result of barrier height set to 0.3 eV with Gaussian doping profile of junction depth set to 100 nm and peak concentration set to 5×10^{17} cm^{-3}……..45

Table 3-6 TFE extraction result of barrier height set to 0.3 eV with Gaussian doping profile of junction depth set to 100 nm and peak concentration set to 5×10^{17} cm^{-3}……..45

Table 3-7 Traditional TE extraction result of barrier height set to 0.3 eV with Gaussian doping profile of junction depth set to 100 nm and peak concentration set to 1×10^{20} cm^{-3}…...……...45

Table 3-8 TFE extraction result of barrier height set to 0.3 eV with Gaussian doping profile of junction depth set to 100 nm and peak concentration set to 1×10^{20} cm^{-3}……..45

Table 3-9 Traditional TE extraction result of barrier height set to 0.3 eV with Gaussian doping profile of junction depth set to 20 nm and peak concentration set to

5×10^{17} cm^{-3}……46

Table 3-10 TFE extraction result of barrier height set to 0.3 eV with Gaussian doping profile of junction depth set to 20 nm and peak concentration set to 5×10^{17} cm^{-3}……..46

Chapter 4

Table 4-1 Traditional TE extraction results of PtSi/p-Si Schottky junction without BF_2^+ ion implantation……63

Table 4-2 TFE extraction results of PtSi/p-Si Schottky junction without BF_2^+ ion implantation……63

Table 4-3 Traditional TE extraction results of NiSi/p-Si Schottky junction without BF_2^+ ion implantation……63

Table 4-4 TFE extraction results of NiSi/p-Si Schottky junction without BF_2^+ ion implantation……64

Table 4-5 TFE extraction results of PtSi/p-Si Schottky junction with BF_2^+ ion implantation at a dose of 1×10^{12} cm^{-2}……..64

Table 4-6 TFE extraction results of NiSi/p-Si Schottky junction with BF_2^+ ion implantation at a dose of 1×10^{12} cm^{-2}……..64

List of Figures

Chapter 1

Fig.1-1 Process of the Schottky barrier formation. (a) Neutral materials separated from each other and (b) electrical equilibrium situation after the contact has been made…….....12

Fig.1-2 Schematic diagram of Fermi-level pinning effect. Electron energy band diagrams of n-type semiconductor with surface states……..12

Fig.1-3 Image force barrier lowering effect. The actual Schottky barrier height lowers down due to the image potential energy……...….13

Fig.1-4 Conducting mechanisms of the Schottky barrier. (1) is the TE mechanism, (2) is the FE mechanism, (3) is the recombination process in the space-charge region and (4) is the hole injection from the metal to the semiconductor……13

Fig.1-5 Example of current-voltage method. Forward current density versus applied voltage, and the barrier height could be extracted from the intercept value..14

Fig.1-6 Example of capacitance-voltage method. The barrier height could be extracted from the intercept at the voltage axis…….14

Fig.1-7 Setting of the photoelectric method. The electron in the metal is excited by heat and penetrates the barrier……...……15

Fig.1-8 Example of photoelectric method. The measured data with low photon energy is interfered with the carrier excited by heat, so the barrier height is extracted by the data with high photon energy……..15

Fig.1-9 Example of activation energy method. The barrier height could be extracted from the slope in this Arrhenius plot……..16

Chapter 2

Fig.2-1 Thermionic-field emission schematic diagram. Holes in the metal are thermally activated and penetrating the Schottky barrier…….....26

Fig.2-2 Extraction flow of TFE method. This procedure is realized by the math tool MATLAB……27

Fig.2-3 Gaussian doped profiles of the simulation. (a) The peak concentration is set to 5×10^{17} cm^{-3}, and the depth of the profile is set to 20 nm (b) The peak concentration is set to 5×10^{17} cm^{-3}, and the depth of the profile is set to 100 nm……..28

Fig.2-4 Energy band diagrams of the simulation. (a) Constant doping profile, the substrate doping concentration is set to 3×10^{15} cm^{-3} (b) Gaussian doped profile, the substrate doping concentration is set to 3×10^{15} cm^{-3}, peak concentration is 5×10^{17} cm^{-3}, and the depth is 100 nm (c) Gaussian doped profile, the substrate doping concentration is set to 3×10^{15} cm^{-3}, peak concentration is 1×10^{20} cm^{-3}, and the depth is 100 nm (d) Gaussian doped profile, and the substrate doping concentration is set to 3×10^{15} cm^{-3}, peak concentration is 5×10^{17} cm^{-3}, and the depth is 20 nm (e) Gaussian doped profile, and the substrate doping concentration is set to 3×10^{15} cm^{-3}, peak concentration is 1×10^{20} cm^{-3}, and the depth is 20 nm.....31

Fig.2-5 Device configuration of Metal/SiC Schottky junction……32

Fig.2-6 Device configuration of Metal/Si Schottky junction with carbon ion implantation……...……32

Fig.2-7 Device configuration of Metal/Ge Schottky junction……..33

Fig.2-8 Device configurations of Metal/p-Si Schottky junction with BF2 ion implantation (a) PtSi/p-Si (b) NiSi/p-Si…...……..……34

Fig.2-9 The chamber of the probe station Lake Shore CPX-VF……..……34

Chapter 3

Fig.3-1 Electrical characteristics are simulated by Sentaurus with constant doping profile and metal work function set to 4.55 eV. Temperature ranges from 100 to 300 K……..47

Fig.3-2 Characteristics difference at the temperature of 300 K between the TFE model and the TCAD tool. The SBH is set to 0.5 eV, and the doping concentration is set to $3x10^{15}$ cm^{-3}……47

Fig.3-3 Electrical characteristics are simulated by Sentaurus with constant doping profile and metal work function set to 4.35 eV. Temperature ranges from 100 to 300 K……..48

Fig.3-4 Extracted SBHs with TE model and TFE model for uniformly doped cases..48

Fig.3-5 Electrical characteristics are simulated by MATLAB with TFE model. The barrier height is set to 0.3 eV and the temperature is set to 100 K. Doping concentration ranges from 1×10^{15} to 1×10^{17} cm-3……...…….49

Fig.3-6 Electrical characteristics are simulated by Sentaurus with Gaussian doping profile and metal work function set to 4.35 eV. The junction depth of Gaussian profile is set to 100 nm and the peak concentration is set to 5×10^{17} cm^{-3}. Temperature ranges from 100 to 200 K……...…….49

Fig.3-7 Electrical characteristics are simulated by Sentaurus with Gaussian doping profile and metal work function set to 4.35 eV. The junction depth of Gaussian profile is set to 100 nm and the peak concentration is set to 1×10^{20} cm^{-3}. Temperature ranges from 100 to 200 K…...…….50

Fig.3-8 Extracted SBHs with TE model and TFE model for Gaussian doped case. The junction depth is set to 100 nm and the peak concentration is set to 5×10^{17} cm^{-3}……50

Fig.3-9 Extracted SBHs with TE model and TFE model for Gaussian doped case. The

junction depth is set to 100 nm and the peak concentration is set to 1×10^{20} cm^{-3}…….51

Fig.3-10 Electrical characteristics are simulated by Sentaurus with Gaussian doping profile and metal work function set to 4.35 eV. The junction depth of Gaussian profile is set to 20 nm and the peak concentration is set to 5×10^{17} cm^{-3}. Temperature ranges from 100 to 200 K…...…….51

Fig.3-11 Electrical characteristics are simulated by Sentaurus with Gaussian doping profile and metal work function set to 4.35 eV. The junction depth of Gaussian profile is set to 20 nm and the peak concentration is set to 1×10^{20} cm^{-3}. Temperature ranges from 100 to 200 K……....52

Fig.3-12 Extracted SBHs with TE model and TFE model for Gaussian doped case. The junction depth is set to 20 nm and the peak concentration is set to 5×10^{17} cm^{-3}……...…….52

Chapter 4

Fig.4-1 Electrical characteristics of Ni/n-SiC Schottky junction are measured at temperature of 423 and 448 K, including the extraction results by both TE and TFE model……...65

Fig.4-2 Electrical characteristics of Ti/n-SiC Schottky junction are measured at temperature of 300 K, including the extraction results by both TE and TFE model……..65

Fig.4-3 Electrical characteristics of NiSi/n-Si Schottky junction with carbon ion implantation are measured at temperature of 300, 325, and 325 K, including the extraction results by both TE and TFE model……...……..66

Fig.4-4 SIMS measurement before silicide formation shows the high concentration of carbon ion near the Schottky junction. SRP measurement shows that the carrier concentration near the junction is only about 10^{18} cm^{-3}…….66

Fig.4-5 Electrical characteristics of NiGe/n-Ge Schottky junction are measured at temperature of 300 K, including the extraction results by both TE and TFE model……..67

Fig.4-6 Electrical characteristics of PtSi/p-Si Schottky junction without ion implantation are measured at the temperature from 100 to 225 K…...…….67

Fig.4-7 Electrical characteristics of NiSi/p-Si Schottky junction without ion implantation are measured at the temperature from 125 to 300 K……...….68

Fig.4-8 Electrical characteristics of PtSi/p-Si Schottky junction with BF_2^+ ion implantation at a dose of 1×10^{12} cm^{-2} are measured at the temperature from 100 to 225 K……..68

Fig.4-9 Electrical characteristics of NiSi/p-Si Schottky junction with BF_2^+ ion implantation at a dose of 1×10^{12} cm^{-2} are measured at the temperature from 100 to 300 K……..69

Fig.4-10 Electrical characteristics of Metal/p-Si Schottky junction with BF2+ ion implantation at a dose of 6×10^{12} cm^{-2} are measured at the temperature from 100 to 300 K (a) PtSi/p-Si: implantation is at a dose 6×10^{12} cm^{-2} (b) NiSi/p-Si: implantation is at a dose 6×10^{12} cm^{-2} (c) PtSi/p-Si: implantation is at a dose 3×10^{13} cm^{-2} (d) NiSi/p-Si: implantation is at a dose 3×10^{13} cm^{-2}..71

Fig.4-11 The temperature dependence of the BH0 without considering the IFBL Effect……..71

Fig.4-12 Illustration of the Fermi energy level and the donor-like interface state density before metal contact……..72

Fig.4-13 Illustration of the charge distribution in the Schottky junction……72

Chapter 1

Introduction

1-1 Fundamental Properties of Schottky Barrier

1-1.1 Schottky Barrier

In 1874, F. Braun has reported the rectifying nature of metallic contacts on iron, copper, and lead sulfide crystal [1]. This is the origin of the metal-semiconductor junction but still far from complete, because their performance is perhaps highly process dependent. But in early 1920s it had been subsequently replaced by vacuum diode. Until the Second World War the point contact diode again became important because of the demand of high frequency converter and low-level microwave detector diode. All these developments are given in the classic book of Torrey and Whitmer [2]. But the contact proved highly unreliable then, it has much superior characteristics nowadays. The significant study toward understanding the rectifying action of metal-semiconductor contact was realized by Schottky and others [3]. Schottky and Mott then explained the mechanism of barrier formation and proposed models for calculating the SBH and the shape of barrier. Till the Second World War, the current transport over the barrier named thermionic emission has been proposed by Bethe [4].

When a metal is contacted with a semiconductor, a potential barrier forms at the metal-semiconductor interface which arises from the separation of charges such that a high-resistance region is created in the semiconductor [5]. The barrier formation process is illustrated in Fig.1. Fig.1-1(a) shows the energy band diagram of an n-type semiconductor with work function $q\phi_s$, which is defined because the Fermi level in the semiconductor varies with the doping concentration, and a metal with work

function $q\phi_m$, which has a volume contribution due to the periodic potential of the crystal lattice and surface contribution due to the existence of a dipole layer. In n-type semiconductor, $q\phi_s$ is equal to $q\chi + q\phi_n$, where $q\chi$ is electron affinity of semiconductor and $q\phi_n$ is the difference between semiconductor Fermi level and conduction band edge. What if in p-type semiconductor, $q\phi_s$ is equal to $q\chi + \varepsilon_g - q\phi_p$, where ε_g is the band gap of semiconductor and $q\phi_p$ is the difference between semiconductor Fermi level and valence band edge. The energy band diagram in Fig.1-1(a) contains no charge at the surface such that the band structure at the surface is the same as that in the bulk and there is no band bending.

Fig.1-1(b) shows the energy band diagram after the two materials has contacted. After the metal contacted, the Fermi level on two sides must be balanced such that electrical equilibrium can be established: the current flow from the metal to the semiconductor would be equal to the other side at zero bias. Furthermore, the vacuum level at the interface must be continuous, or the electric field would be an infinite value irrationally. Based on these two conditions, the barrier is equal to $q(\phi_m - \chi)$. The electrons on the semiconductor will flow into metal in this state, so the free electron concentration at the interface surface decreases such that the conduction band bends up as shown in Fig.1-1(b). Thus a positive space charge region is established on the semiconductor side and the electrons flow into the metal form a thin sheet of negative charge. What if in p-type semiconductor, the electrons would be replaced by holes because the major carrier would not be electrons such that a negative charge layer forms at the semiconductor surface, and the electrons at the metal side would be recombined by holes to form a thin positive charge layer.

The potential barrier forms between the semiconductor and the metal here is

named Schottky barrier which is a main factor to determined current transport at the metal-semiconductor contact.

1-1.2 Fermi-level Pinning

The description above is the ideal case of Schottky barrier, but indeed there is other factor to determine how Schottky barrier forms. Fermi-level pinning is one effect to stand for, and it is a major challenge to decrease SBH nowadays. This phenomenon, which SBH is insensitive to metal work function in covalently bonded semiconductors, was first explained by Bardeen [6] who pointed out that localized surface states would determine the SBH. The surface atom has one broken covalent bond which is also named dangling bond. Dangling bonds would generate energy states at the surface of semiconductor in the forbidden gap. The surface states are usually continuously distributed in the band gap and characterized by a charge neutrality level $q\phi_0$, which is shown in Fig.1-2 [7]. If the SBH is independent of the metal work function, it can be written by $q\phi_B = \varepsilon_g - q\phi_0$. Fermi-level pinning effect is mainly caused from metal induced gap states (MIGS) [8-10] and interface dipoles [11, 12], but more details are not concluded here, because this study give more focus on how to measure the SBH.

1-1.3 Barrier Lowering

The other effect which would change SBH is the image force barrier lowering, which is due to the electric field in the depletion region. This effect can be easily understood by Fig.1-3. There is an electric field perpendicular to the metal surface, so an electron must be subjected to the field at a distance x from the surface. The field can be calculated as an image force which is $q^2/4\pi\varepsilon_d(2x)^2$, so the electron has a

negative potential energy $-q^2/16\pi\varepsilon_d x$ which should be added to the barrier energy to obtain the total energy of the electron. The magnitude $\Delta\phi_B$ of the image force barrier lowering is given by

$$\Delta\phi_B = \left[\frac{q^3 N_d}{8\pi^2\varepsilon_d^2\varepsilon_s}(V_i - V)\right]^{1/4} \quad [13].$$

Here N_d is the doping concentration of the semiconductor, V is the applied voltage, and ε_d is the image force permittivity which may be different from the static permittivity ε_s. The image force barrier lowering resulted from the field produced by electrons. So when the SBH is measured by a method without movement of the electrons over the barrier, the obtained $\Delta\phi_B$ will be zero.

1-2 Potential Application of Low Schottky Barrier

As the semiconductor device scales down, contact resistances between metal and source/drain (S/D) become a critical problem due to the scaled contact area. The equation of contact resistance is given as $R_c = \rho_c / A_c$, where R_c is the contact resistance, A_c is the contact area and ρ_c is the specific contact resistance which is determined by the contact materials. The equation above shows that the contact resistance would be larger as the contact area becomes smaller. Even though the channel could generate sufficient carriers to raise the theoretical driving capability, the real driving current would be degraded due to the serial resistances at the contacts between metal and S/D, so how to reduce the contact resistance becomes an urgent issue for the aggressive scaling in nowadays.

At the other side, Schottky S/D becomes a possible solution in very large scale integration (VLSI) technology in the future. In order to achieve highly doped junctions, steep lateral profiling and low contact specific resistance, a brand new idea

that integrates Schottky S/D in metal-oxide-semiconductor field effect transistor's (MOSFET) architectures have been proposed [14]. This new idea have inherently solved the problem that control of S/D doping for short gate geometries. Recent publication [15, 16] have shown the need for extremely low Schottky barriers (~0.1 eV) to obtain current drives that compete with highly doped S/D MOSFETs.

Platinum silicide on p-type silicon (PtSi/p-Si) substrate is a good example for low Schottky barrier which has a typical SBH to holes around 0.22-0.25 eV according to the literature [17-20]. The most inviting advantage of PtSi is that specific contact resistance can reach an ultra-low value such that the rectifying effect at the metal-semiconductor junction no longer exists. Specific contact resistance can be described as $\rho_c = R_c \times A_c \propto \exp\left[\frac{2\sqrt{\varepsilon m^*}}{\hbar}\left(\frac{\phi_{bn}}{\sqrt{N_D}}\right)\right]$, where R_c is contact resistance, A_c is contact area, ε is dielectric constant, and m^* is the effective mass of the electron. As the SBH getting lower, the specific contact resistance performs even like an Ohmic contact. So this study focuses on how to extract the SBH of PtSi on p-type silicon substrate by a brand new method

1-3 Conducting Mechanism in the Schottky Barrier

Before starting to introduce the traditional extraction methods of the SBH, it is necessary to understand the current transport of the barrier, because most measurements of the SBH are based on the behavior of the conducting carriers. There are four main conducting mechanisms: (a) thermionic emission (TE) (b) field emission (FE) (c) carrier recombination (d) minority carrier injection. All these four mechanisms are described in Fig.1-4. In general case, (c) and (d) take very small part

of the total current, so this study only discusses (a) and (b) for extracting the SBH. TE is the most popular mechanism in extracting the SBH, and it can be written in

$$I = AA^{*}T^{2}\exp\left(\frac{-\phi_b}{kT}\right)\left[\exp\left(\frac{qV}{kT}\right)-1\right],$$

where A is the diode area and A^{*} is the Richardson constant which is a variable of the effective mass of the conducting carrier [21]. The most treatment is completed by Crowell and Sze [22], FE is the other dominant mechanism to make up the insufficiency of TE. When barrier is thin enough, the carrier in semiconductor would pass through the barrier by tunneling through it. This situation can be realized in a highly doped semiconductor material, because higher doping concentration would cause higher electric field in metal-semiconductor contact. This study focuses more on how to combine TE and FE to measure the SBH, because the carrier would not stay at the band edge but thermally excited to a higher level. When a carrier is thermally excited to a higher level, it may see a lower barrier than when it stays at the band edge. Then the carrier would pass through the lower barrier by FE, the two step of the conducting mechanism is known as thermionic field emission (TFE).

1-4 Traditional Extraction Method of the Schottky Barrier

After realizing the main conducting mechanisms, following introduces the extraction methods of the SBH. There are also four main methods: (a) current-voltage method, (b) capacitance-voltage method, (c) photoelectric current method, and (d) activation energy method.

1-4.1 Current-Voltage Method

The current on the Schottky barrier is due to thermionic emission, so the SBH can be extracted by the equation

$$J = A^{*}T^{2}\exp\left(\frac{-\phi_b}{kT}\right)\left[\exp\left(\frac{qV}{nkT}\right)-1\right],$$

where n is the diode ideality factor, which is caused by the image force barrier lowering mechanism and the other non-ideal factors such as surface defects and interfacial layer. Because the barrier lowering would be varied by the applied voltage, the exact SBH would be different if the applied voltage changed, so we need to take the ideality factor to modify the slope in current-voltage plot. Assuming the measured data are shown in Fig.1-5, we take some points which is in excess of 3kT/q such that exponential term would be large enough and rewrite the equation into

$$\ln(J) = \ln\left(A^{*}T^{2}e^{-\frac{\phi_b}{kT}}\right)+\frac{qV}{nkT}.$$

Knowing the Richardson constant A^{*} and the temperature, the SBH value can be extracted by extrapolating the straight line to V=0 in Fig.1-5.

1-4.2 Capacitance-Voltage Method

This method is based on the capacitance in semiconductor at reverse bias, and the SBH can be extracted by the equation

$$\frac{1}{C^2} = \frac{2}{q\varepsilon_S N_D}\left(V_{bi} - V - \frac{kT}{q}\right).$$

By the plot of $1/C^2$ versus V_R which is shown in Fig.1-6, the value of V_{bi} can be extrapolated, where V_{bi} is equal to V_x+kT/q. V_x stands for the applied voltage should be given for flat band in the semiconductor, and kT/q is a correction term for flat band because the band bending would not be zero even the applied voltage is given. Then we know the barrier can be written in the following equation

$$\phi_b = V_x + V_o + \frac{kT}{q} \quad \text{and} \quad V_o = \frac{kT}{q}\times \ell n\left(\frac{N_C}{N_D}\right),.$$

where V_0 is the energy difference between Fermi-level and band edge. By adding this term the real SBH can be calculated, where T and N_C are known, N_D can be calculated from the slope of the plot. More comprehensive discussion of this method has been given by Goodman [23].

1-4.3 Photoelectric Method

This method is the most accurate and direct method of determining the SBH. As shown in Fig.1-7, by illuminating monochromatic light on the metal, electrons on the metal would be excited to surpass the barrier such that photocurrent would be generated. The photocurrent can be formulated in the following equation

$$I_{ph} = B(h\nu - q\phi_b)^2,$$

where B is a constant, h is Planck's constant, and ν is frequency. We can extract the SBH by extrapolating the plot of $I_{ph}^{0.5}$ versus $h\nu$ as shown in Fig.1-8. In this plot some limitations in this method can be figured out. First, the photo energy could not be larger than the band gap of the semiconductor, or there would be other current by generation current mechanism in the measurement. Second, if the photo energy is not large enough, the measured data would not be linearly proportional to the photo energy, because the electrons in the metal would be thermal excited so we could not distinguish that the current is generated by the photo or the heat of temperature.

1-4.4 Activation Energy Method

This method is based on the current-voltage characteristic, by changing the variable of V. In case A^* is unknown, the SBH still could be extracted by the thermionic emission model. If we fix the applied voltage and draw the plot of $\ln(J_0/T^2)$ versus 1/T as shown in Fig.1-9.

$$\ln\left(\frac{J_0}{T^2}\right)=\ln\left(A^*\right)-\frac{q(\phi_{Bn}-V)}{k}\left(\frac{1}{T}\right)$$

The equation above shows that the slope in the plot would contain the information of the SBH. The applied voltage is known, so the SBH still could be calculated.

1-5 Motivation

After introducing the traditional extraction methods of the SBH, the study now focuses on the issue of the low SBH. Because all this four methods have their limitations, the SBH in the low barrier cases could not be extracted. For current-voltage method and activation energy method, the band bending at forward bias in the low barrier cases would be unobvious. That is, the current in measurement would be dominated by parasitic resistance, so there could not be sufficient data to calculate the SBH in the linear region of the plot. For the capacitance-voltage method, the current at reverse bias in the low barrier cases is too large to measure reliable capacitance value. For photoelectric method, the barrier is too low to distinguish the current generated by photon or by heat. According to these problems, it is known that there is still no precise method to extract the SBH in the low barrier cases. Most of the literature proposed recently used the effective SBH to show how low the SBH they have achieved, but the values are not correct indeed [24-28]. Because the measured I-V characteristics are not thermionic emission dominant, using these extraction methods could not obtain the valid information of the SBH.

The exact SBH determines what conducting mechanism dominates the Schottky barrier, but most traditional methods give the effective values meaninglessly. For example, the current density could be raised by adding donors (or acceptors) into the semiconductor, and the tunneling current (FE) would be the dominant mechanism as the barrier gets thinner. However, the traditional method only takes TE model into

consideration, and the extracted values would be effectively lowered down. The results give wrong information, and what did happen after the fabrication process would be never known. In order to avoid such situations, this study proposes a new method which contains more conducting mechanisms.

First, since the information of C-V characteristics of the low barrier is not reliable, the information of I-V characteristics is still necessary. Second, the information of I-V characteristics at forward bias is not sufficient, so the information at reverse bias is taken into consideration such that the image force barrier lowering effect would be more obvious. Such method has been proposed [29], and the conducting mechanism of the Schottky barrier at reverse bias is known as TFE model. But there is still one other problem, the conducting mechanism at reverse bias is no longer a simple TE model, so the SBH could not be extracted by a simple formula. The conducting mechanism of the Schottky barrier at reverse bias named TFE model is a too complicated integral to calculate by hand, so program computing is adopted to replace this hard work. By programing a procedure in MATLAB, the measured data could be fit with theoretical data to extract the information of the Schottky barrier.

1-6 Organization

The first chapter is the introduction including the fundamentals of the Schottky barrier, the advantage and the feasibility of the low barrier cases, traditional extraction methods, and then proposing a new method to overcome the problem of the traditional methods. Chapter 2 shows the procedure of this new method, simulation setting, experiment setting, and process flow.

Simulation result is discussed in Chapter 3. First, the feasibility of this new method is verified by the simulation data. However, the simulation tool is not so intact

for the real cases, so the procedure has been verified again by the real Schottky barrier contact with silicon, silicon carbide, and germanium substrates in Chapter 4. To achieve the goal of extracting the exact low SBH cases, platinum silicide on p-type silicon substrates is also studied in the same chapter. Finally the feasibility of this new method has been verified again in the exact low barrier cases. The last chapter is the summary and future works of this thesis.

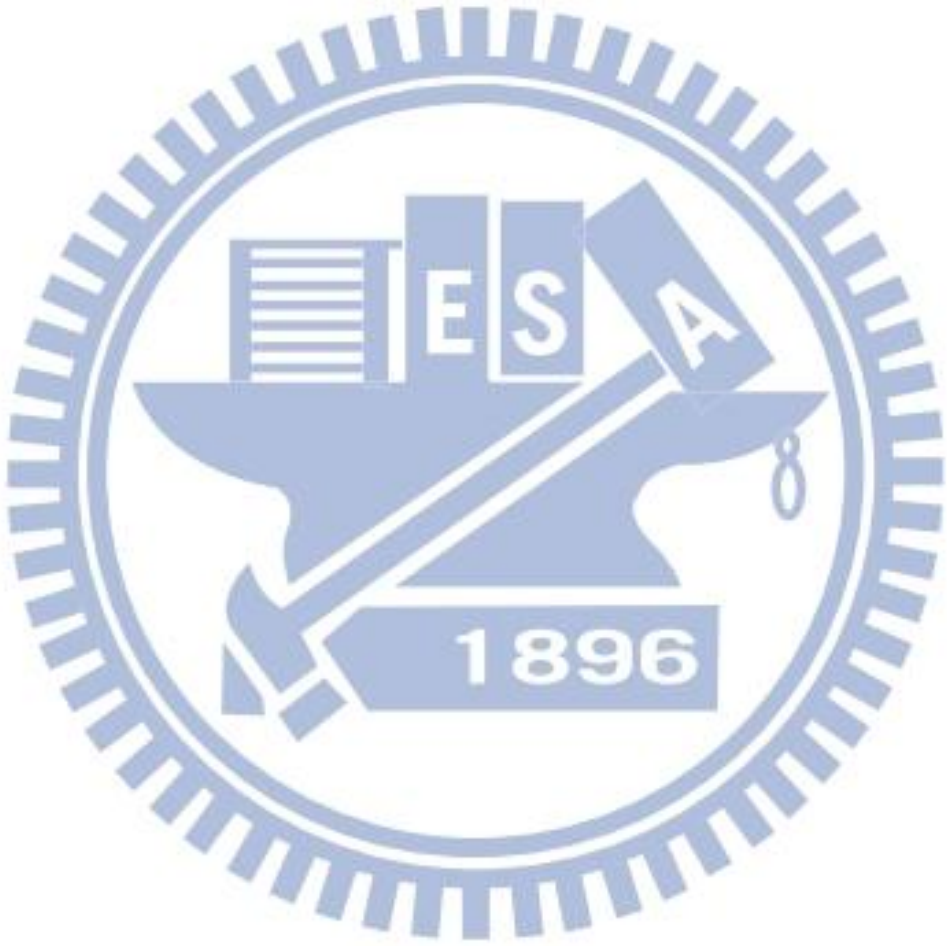

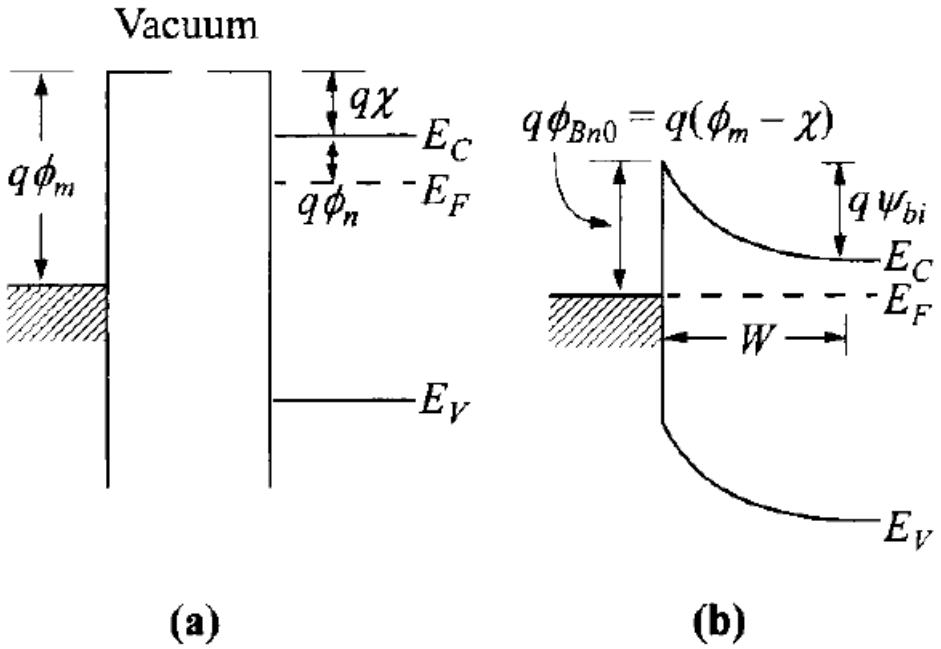

Fig.1-1 Process of the Schottky barrier formation. (a) Neutral materials separated from each other and (b) electrical equilibrium situation after the contact has been made [13].

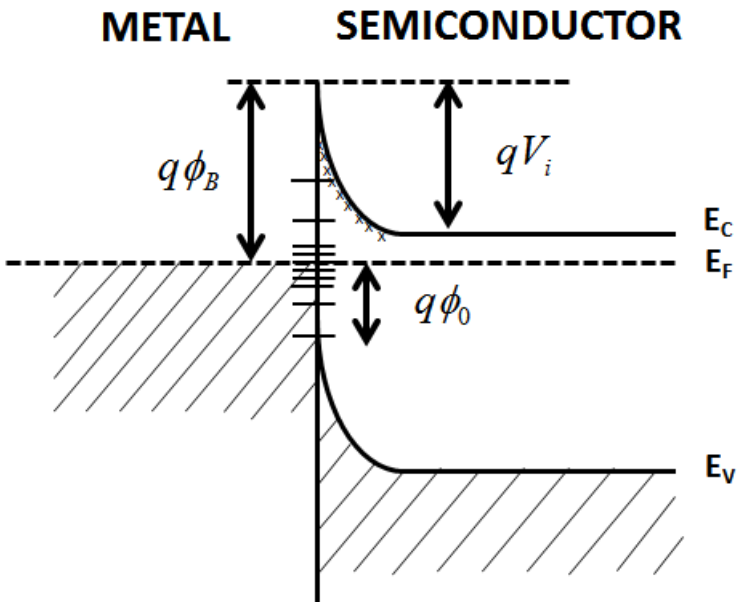

Fig.1-2 Schematic diagram of Fermi-level pinning effect. Electron energy band diagrams of n-type semiconductor with surface states.

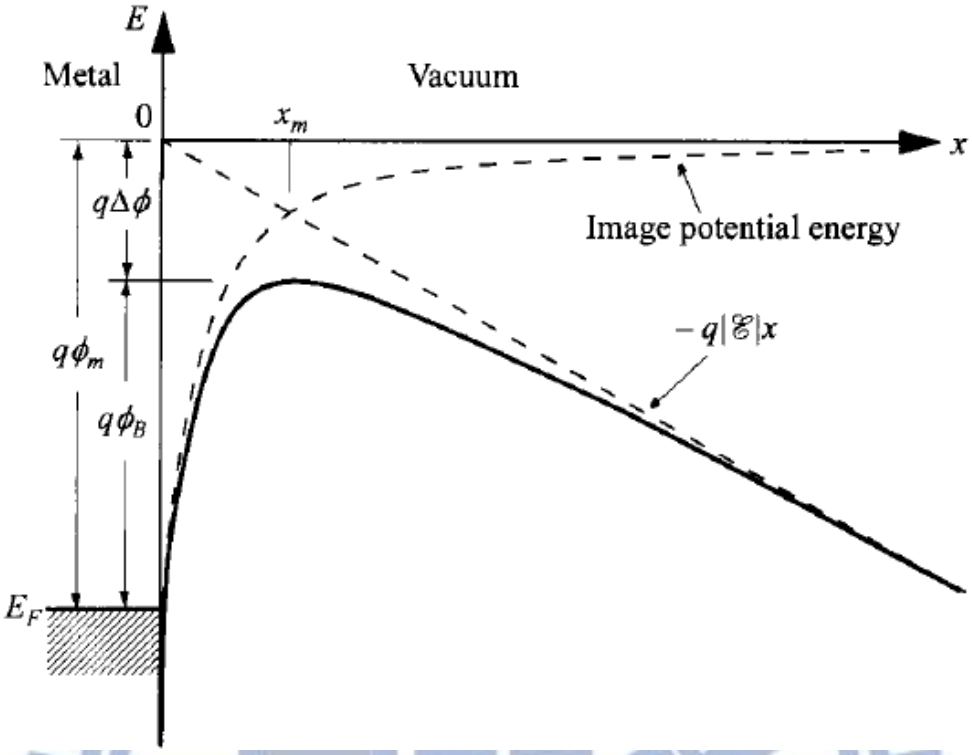

Fig.1-3 Image force barrier lowering effect. The actual Schottky barrier height lowers down due to the image potential energy [17].

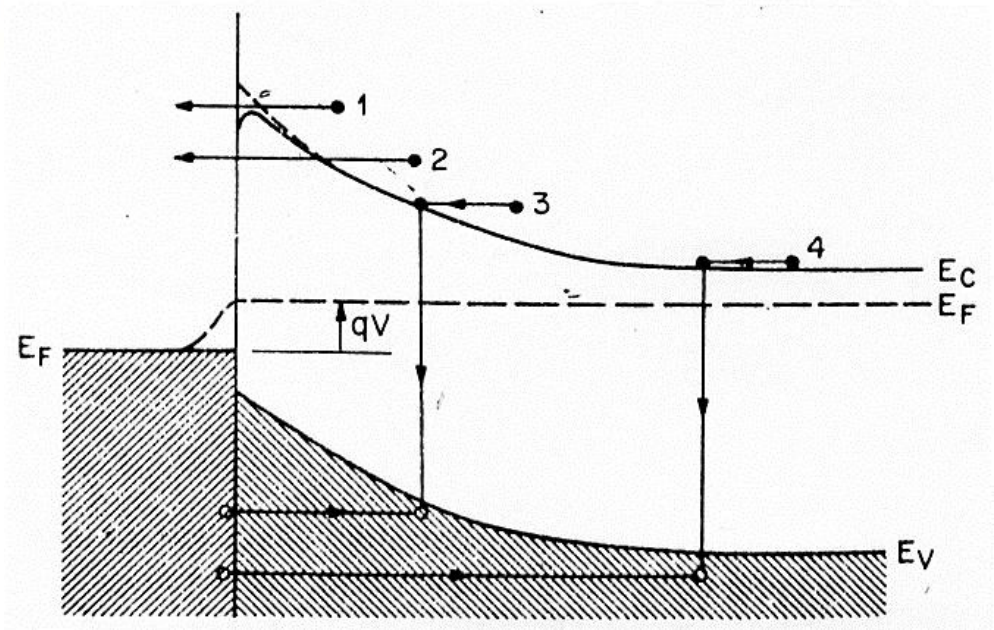

Fig.1-4 Conducting mechanisms of the Schottky barrier. (1) is the TE mechanism, (2) is the FE mechanism, (3) is the recombination process in the space-charge region and (4) is the hole injection from the metal to the semiconductor [17]

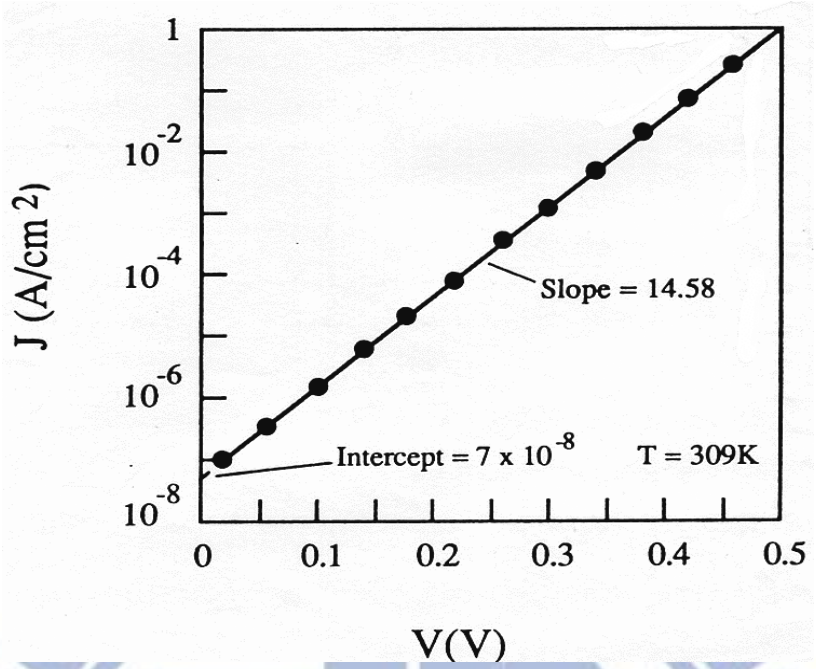

Fig.1-5 Example of current-voltage method. Forward current density versus applied voltage, and the barrier height could be extracted from the intercept value [17].

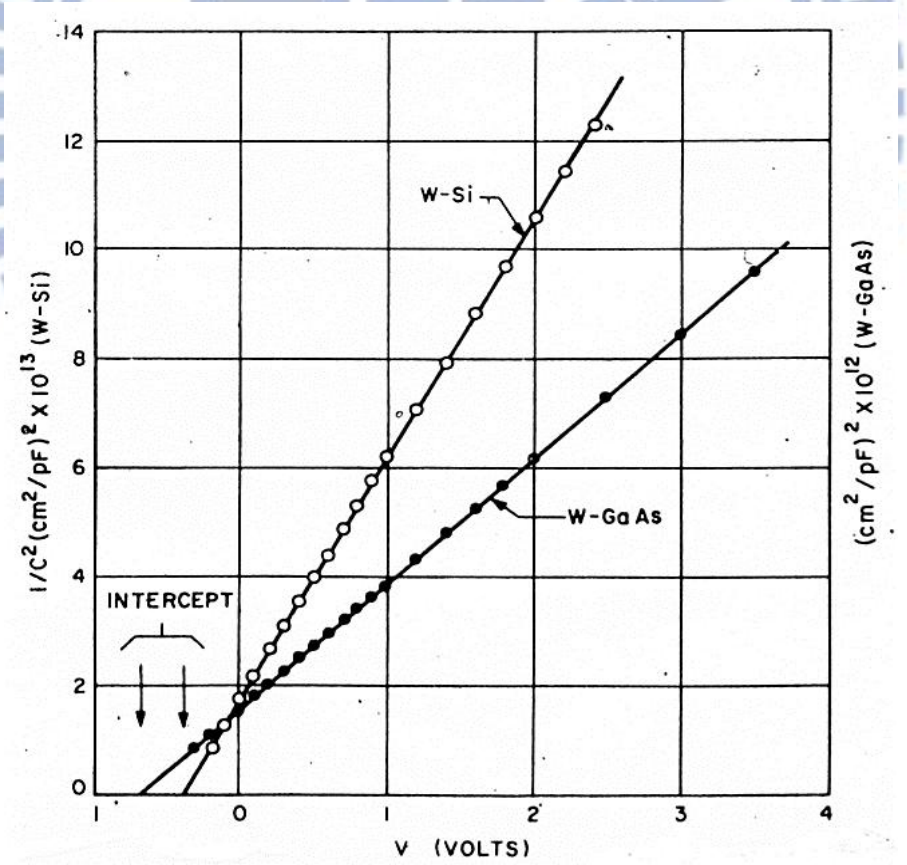

Fig.1-6 Example of capacitance-voltage method. The barrier height could be extracted from the intercept at the voltage axis [17].

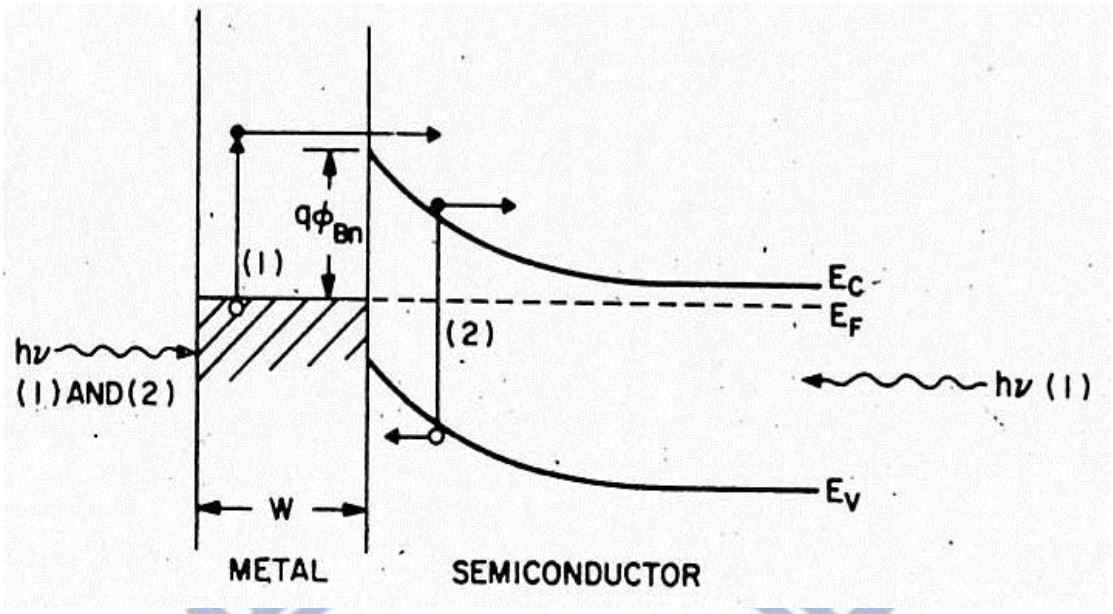

Fig.1-7 Setting of the photoelectric method. The electron in the metal is excited by heat and penetrates the barrier [17].

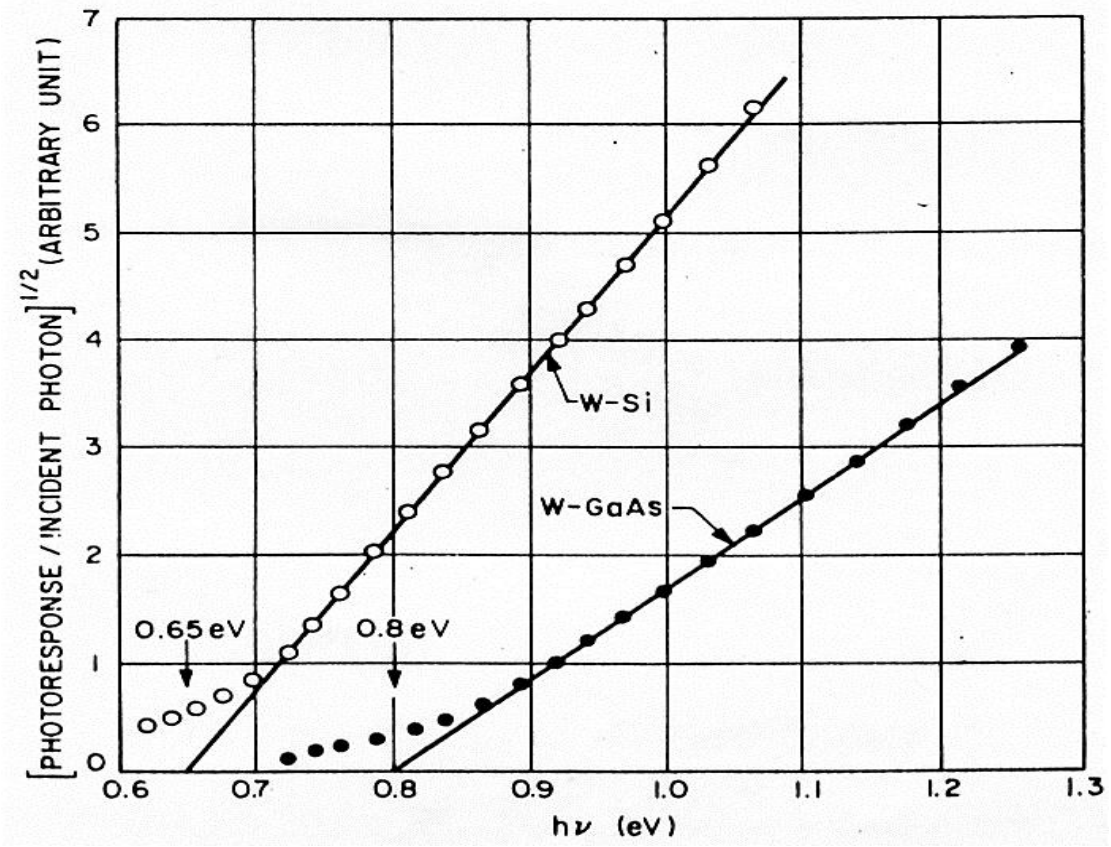

Fig.1-8 Example of photoelectric method. The measured data with low photon energy is interfered with the carrier excited by heat, so the barrier height is extracted by the data with high photon energy [17].

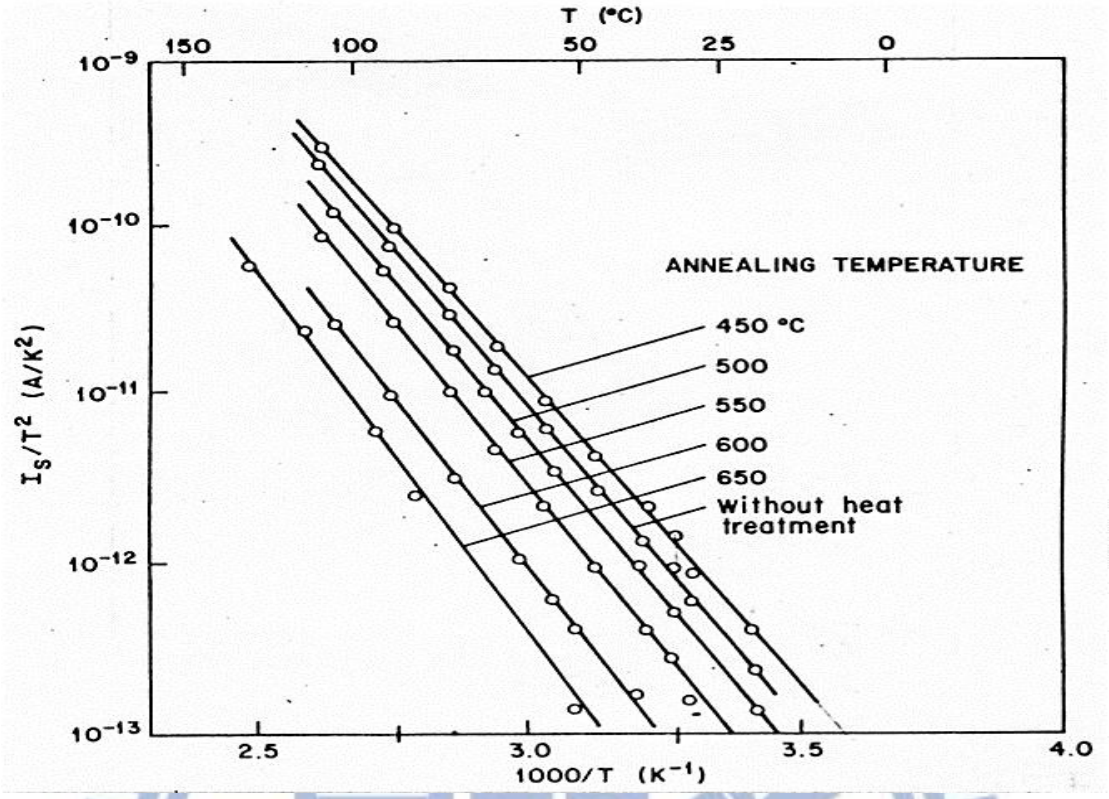

Fig.1-9 Example of activation energy method. The barrier height could be extracted from the slope in this Arrhenius plot [17].

Chapter 2

Extraction Model and Experiments

2-1 Extraction Model

The proposed new extraction method is based on the conducting current under reverse bias of the Schottky barrier, so the TFE model which has been introduced in chapter 1 is adopted in this thesis. The carriers would be thermally excited to a higher energy and pass through the lower barrier, which is shown in Fig.2-1. The TFE model derived under the WKB approximation can be expressed as

$$J_R = J_{R0}\left[1+\frac{E_b}{kT}\int_0^1 \exp\left\{\frac{-E_b}{kT}\left[\alpha-1+\frac{kT}{E_{00}}y(\alpha)\right]\right\}d\alpha\right] \quad [24]$$

where E_b =q(ϕ_{bp} - ϕ_s + V_R) is the band bending in the semiconductor, ϕ_{bp} is the Schottky barrier, ϕ_s is the energy difference between Fermi level and valence band edge, and V_R is the reverse bias. The J_{R0} shown in the following equation stands for the reverse saturation current of pure thermionic emission.

$$J_{RO} = A\times T^2 \times \exp\left(\frac{-q\phi_{bp}}{kT}\right)$$

The parameter E_{00} is a property of the semiconductor through its dielectric constant ε_s, the effective mass of carriers m^*, and the doping concentration N. The ratio kT/E_{00} would decide whether the dominant mechanism is TE or FE. The FE model dominates the conducting mechanism at reverse bias in the Schottky barrier when $kT/E_{00} \approx 1$, while $kT/E_{00} >> 1$ TE is the most significant mechanism.

$$E_{00} = \frac{qh}{4\pi}\left[\frac{N}{m^*\varepsilon_s}\right]^{1/2}$$

The function $y(\alpha)$ responds the transformation of the integration of TE/FE over distance into one over energy [30]. It can be defined by

$$y(\alpha)=(1-\alpha)^{1/2}-\alpha\ln\left[\frac{1+(1-\alpha)^{1/2}}{\alpha^{1/2}}\right]$$

Above all we have just introduced the conducting mechanism in this extraction method, now we take other factors into consideration. The first one must be considered is the IFBL effect introduced in Chapter 1.

$$\Delta\phi_B=\left[\frac{q^3N_d}{8\pi^2\varepsilon_d^2\varepsilon_s}(V_i-V)\right]^{1/4}$$

The second is the parasitic resistance which can be extracted at forward bias, because we have to deduct the voltage drop due to the parasitic resistance from the measurement. For calculating the energy difference between the Fermi level and band edge, we need to take an appropriate model of density of states (DOS) into consideration, so we take the DOS model from Synopsys Sentaurus [26].

$$N_C(T)=2\left(\frac{2\pi m_e k_B T}{h^2}\right)^{3/2} \qquad N_V(T)=2\left(\frac{2\pi m_h k_B T}{h^2}\right)^{3/2}$$

$$m_e/m_0=\left[(6m_t)^2 m_l\right]^{1/3}+mm_e$$

$$m_h/m_0=\left\{\left[\left(a+bT+cT^2+dT^3+eT^4\right)/\left(1+fT+gT^2+hT^3+iT^4\right)\right]^{2/3}+mm_h\right\}$$

The constants a, b, c, d, e, f, g, h, i, m_l, m_t, mm_e, and mm_h in above equations depend on materials. At last, we realized this extraction method by MATLAB and the total extraction procedure is shown in Fig.2-2.

In this procedure, the I-V-T data we measured or simulated is input to a designated excel file and the data will be retrieved while the program is running. Before running this program, it is necessary to declare the semiconductor material and doping type, the parameters of semiconductors are given. Then we set the calculating

ranges of SBH and N. While running this program, the parasitic resistance will be extracted from the I-V-T data at forward bias. The parasitic resistance is extracted by the slope of the linear region in the I-V-T characteristic at high forward bias, and the extracting rule is that the error of the slopes at continual points must be smaller than 1%. Then take advantage of this resistance value to modify the voltage drop at any bias, because the total voltage consists of the voltage drops across the Schottky junction and the parasitic resistance, and only the voltage drop across the Schottky junction should be used to extract the SBH. Afterwards, the program will calculate multiple I-V-T data with the TFE model and the IFBL effect, compare these calculated data with the measured data in the designated excel file, and adjust the SBH and N until the minimum error is obtained.

There are some critical parameter-setting tricks in the extracting procedure to determine the extraction result converged or not. Before running the program, it is necessary to declare the upper and lower bounds of the SBH and N. Improper settings may cause the extracted results incorrect and the results would be at the bound of the settings. In order to prevent this situation, the program has been modified a little bit. The SBH and N are extracted by 4-step: first, the full range is uniformly divided into 10 parts, and the part with the lowest error is found out. This part is then divided into 10 subparts, and the subpart with the lowest error is found out again. The partition procedure repeats 4 times, and each partition would re-allocate the bound ranges of the SBH and N: if the answers are beyond the pre-set bounds, the program will move the bounds to make the answers inside the bound ranges. After four times calculation, the SBH and N have sufficient accuracy. To fit the I-V characteristics from measured one, there is another parameter m^* (effective tunneling mass) needed to be determined. The slope of the leakage current in logarithm scale highly depends on the parameter E_{00}, the higher E_{00} the higher slope. However, the E_{00} value is consisted of $(N/m^*)^{0.5}$,

and it means that the extracted N highly depends on the effective mass for the same E_{00}. What if the m^* settings is 10 times by the real one, and the extracted N is also 10 times by the exact one, so the m^* setting is critical for each case of the different Schottky junctions.

2-2 Simulation Settings

The electrical characteristics of a Schottky junction with different SBHs and doping profiles can be studied by TCAD simulation. In this thesis, Synopsys Sentaurus was used [31]. The thickness of the silicon substrate is fixed at 400μm. The square shape contact area has length 100 μm at each side. The thickness of the metal is set to 50 nm and the resistivity is set to 15 μohm-cm. These two parameters do not affect the simulated results almost.

The simulation tool does not include the metal induced gap states (MIGS) model, so the metal work function is the only parameters to determine the SBH. The SBH is ideal in this simulation tool, so the SBH in n-type semiconductor is equal to $\phi_m - \chi$, and the SBH in p-type semiconductor is equal to $\chi + \varepsilon_g - \phi_m$. In order to fix the SBH at different temperature, the n-type semiconductor is adopted in this thesis, because there is a temperature dependent parameter, the band gap of semiconductor, in the ideal formula for p-type semiconductor.

In this thesis the SBH is set to 0.3 and 0.5 eV, and the substrate doping is set to 3×10^{15} cm^{-3}. Two kinds of doping profiles are considered, one is constant doping profile and the other is Gaussian doping profile. The constant doping is simply the original substrate doping. For the Gaussian doping profile, two junction depths of 20

and 100 nm are used as shown in Fig.2-3. The peak concentrations are set to 5×10^{17} cm^{-3} and 1×10^{20} cm^{-3}. The energy band diagram is shown in Fig.2-4.

2-3 Experiment Settings

The experiments are divided into two parts. In part-1, different metal/semiconductor Schottky junctions, including three different semiconductor substrates, silicon, germanium, and silicon carbide, were used to verify the validity of the proposed extraction procedure. In order to verify that the extracted results are consistent with the traditional TE method, some SBHs should be set high enough, so that we can extract the SBH by forward I-V characteristics. First, Ti and Ni Schottky contacts on n-type silicon carbide (SiC) substrate are adopted, because their SBHs are up to 1 eV [32-38]. Second, we discuss the case of NiSi Schottky contact on n-type silicon substrate. The SBH of this contact is about 0.65 eV [39-42]. The effect of carbon doping on the SBH and N are also studied [43-44]. Finally, we discuss the SBH of NiGe/Ge Schottky contact on n-type germanium substrate. Due to the narrow band gap of germanium and the severe Fermi-level pinning effect, the SBH is around 0.5 eV [45-46]. It can be regarded as a transitive case to the low SBH extraction. The SBH extraction by the TE model at room temperature on this contact has been a considerable difficulty.

In part-2, after the verification of the extraction procedure, SBHs of some low barrier height Schottky contacts were extracted by this procedure. In this part, NiSi and PtSi Schottky contacts on p-type silicon substrate are adopted, because the SBHs of these two contacts are too low, about 0.45 eV and 0.25 eV, respectively [47-50], to be extracted by traditional TE method. On the other hand, the NiSi and PtSi samples with BF_2^+ implantation are also studied. The implantation energy was 30 keV, and the

implant doses were 1×10^{12}, 6×10^{12}, and 3×10^{13} cm^{-2}.

2-4 Device Fabrication

Metal/SiC Schottky contact:

The semiconductor material was n-type SiC substrate with 11-μm-thick epi-layer. After standard RCA clean, a 100-nm-thick SiO_2 capping layer was deposited by PECVD to protect the front side surface during the backside contact process. In order to make backside contact ohmic, a 100-nm-thick Ni layer was deposited on backside and annealed at 1000 °C for 15 minutes by furnace. Before forming front side Schottky contact, the capping oxide was removed by BOE solution, and re-deposited 200-nm-thick isolation SiO_2 layer by PECVD. Contact holes were patterned by conventional optical lithography process, but the photoresist was still remained for metal layer lift-off. A 100-nm-thick metal layer, Ti and Ni were both used, was deposited by sputtering system, and a 300-nm-thick Al layer was coated by thermal coater. After metal layer lift-off, Schottky contacts alloy were carried out by furnace at 500 °C for 5 minutes. The final structure is shown in Fig.2-5.

Metal/Si Schottky contact with carbon ion implantation:

The starting material was (100)-oriented phosphorus-doped Si substrate with a nominal resistivity 2.7~4 ohm-cm. After standard RCA clean, a typical local-oxidation-of-silicon (LOCOS) isolation process was performed. Then, a 70-nm-thick screen oxide layer was thermally grown followed by carbon ion implantation at 40 keV to a dose of 1×10^{15} cm^{-2}. The projected ion range of C ions is 58.7 nm under the Si substrate surface, which is slightly deeper than the final NiSi/Si interface. In order to repairing the defects caused by the ion implantation, the sample

was annealed by a rapid-thermal annealing (RTA) system at 1050 °C for 30 seconds in N_2 ambient. Afterwards, the screen oxide layer was removed by diluted-HF. A 25-nm-thick Ni layer and a 5-nm-thick TiN capping layer were deposited in a sputtering system, and the silicide formation was carried out by a RTA system at 500 °C for 30 seconds. Then, the TiN capping layer and unreacted Ni were selectively etched by a mixture of H_2SO_4:H_2O_2=3:1. Finally, a 300-nm-thick Al was deposited on the wafer backside to form ohmic contact. The final structure is shown in Fig.2-6.

Metal/Ge Schottky contact:

N-type Ge substrate was adopted, and started the device fabrication with several times diluted HF solution clean. Because Ge could be easily oxidized, and GeO_2 is water-soluble, standard RCA clean is not an appropriate clean process. A 200-nm-thick SiO_2 layer was deposited by PECVD, and contact holes were patterned by conventional optical lithography process. After contact holes etching by BOE solution, the photoresist was still retained for metal layer lift-off. In order to form front side Schottky contacts, Ni (15 nm)/TiN (15 nm) layers were deposited by a sputtering system and the metal outside the contact holes was lifted-off. Germanide formation was carried out by a RTA system at 500 °C for 30 seconds, and the residual metal was removed by hot HCl solution. Finally, backside Al layer of 300-nm-thick was deposited by a thermal coater, and the final structure is shown in Fig.2-7.

Metal/Si Schottky contacts with BF_2^+ ion implantation:

The starting material was heavily-boron-doped Si substrate with 4-μm-thick low doping epi-layer. The high doping substrate ($>10^{18} cm^{-3}$) is used to lower the parasitic resistance, and the low doping epi-layer ($\approx 10^{15} cm^{-3}$) is used for Schottky junction formation. Samples were implanted by BF_2^+ ions at 30 keV to the doses of 1×10^{12}, 6

$\times 10^{12}$, and 3×10^{13} cm^{-2}, and activated at 1000°C for 10 seconds. Samples without ion implantation were also retained. After standard RCA clean, 200-nm-thick SiO_2 layer was deposited by PECVD, and contact holes were patterned by lithography. Then, contact holes were etched out by BOE solution, but the photoresist was still remained for metal layer lift-off. Metal layer, both Pt (15 nm) and Ni (15 nm)/TiN (15 nm) layers were used, was deposited by a sputtering system, and the metal outside contact holes was lifted-off. Silicide formation, both PtSi and NiSi, was performed by a RTA system at 500°C for 30 seconds. The unreacted metal was not etched after the silicide formation for both two cases. Finally, backside 20-nm-thick Pt layer was deposited by sputtering system to form good ohmic contact and the final structure is shown in Fig.2-8. The backside metal selection here is critical, because the resistance values of the front side Schottky junctions are very low. Al would not be an appropriate material for backside contact, because its SBH to p-type Si is too high, and the I-V characteristic would be dominant by backside Al contact. Here we selected Pt as the backside metal because of its low SBH to p-type Si.

2-5 Low temperature measurement

To extract the SBH of the above samples, it is necessary to measure the I-V-T characteristics. Most samples could be measured at room temperature, but the PtSi sample and the BF_2^+ implanted samples could not because the junction resistance is too low to measure the rectifying effect at room temperature, and the I-V-T characteristic would be dominated by parasitic resistance. Measurement at low temperature is needed such that the rectifying effect would appear.

Measurement was executed in the probe station of model Lake Shore CPX-VF as shown in Fig.2-9, and the I-V-T characteristics were obtained by the semiconductor

characterization system of model Keithley 4200-SCS. At first, samples were put into the chamber of the probe station, and then lowered the air pressure to about 10^{-5} torr to avoid the solidification of moisture and residual gas molecules. Afterwards, the chamber temperature was lowered to 100 K by liquid N_2 circulation, and the I-V-T characteristics were measured at this temperature. Then the chamber temperature was raised by a step of 25 K for each measurement until the rectifying effect disappeared.

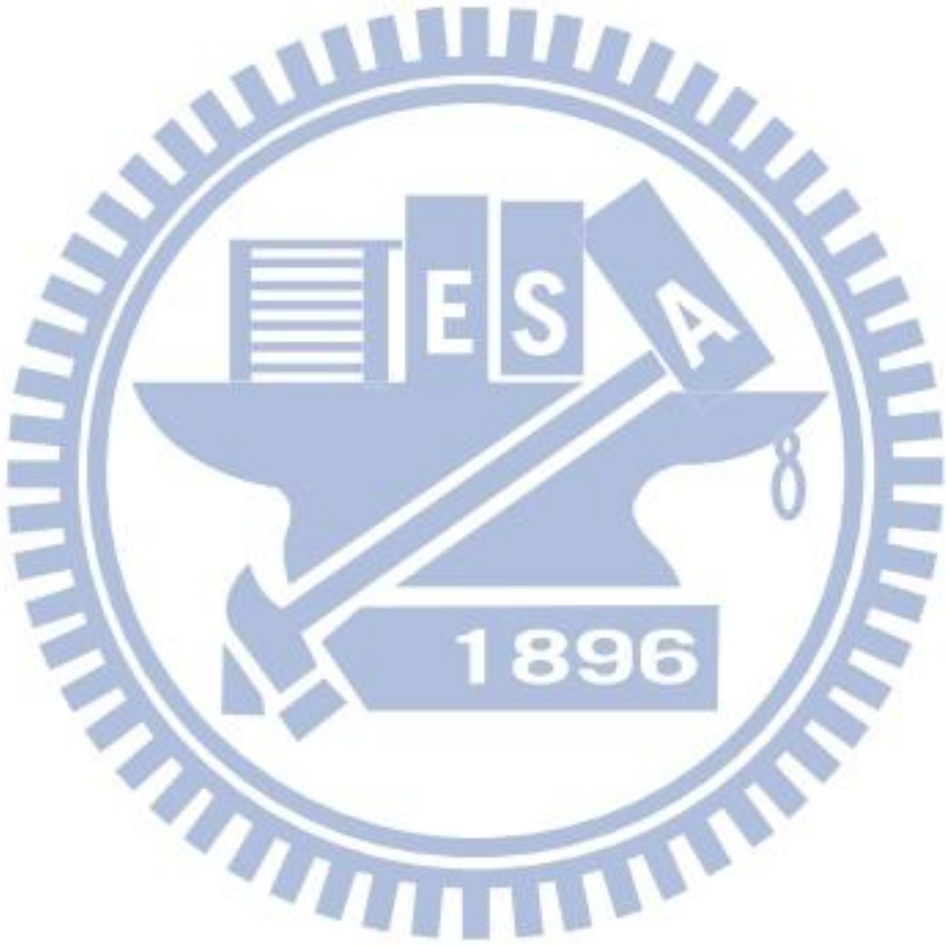

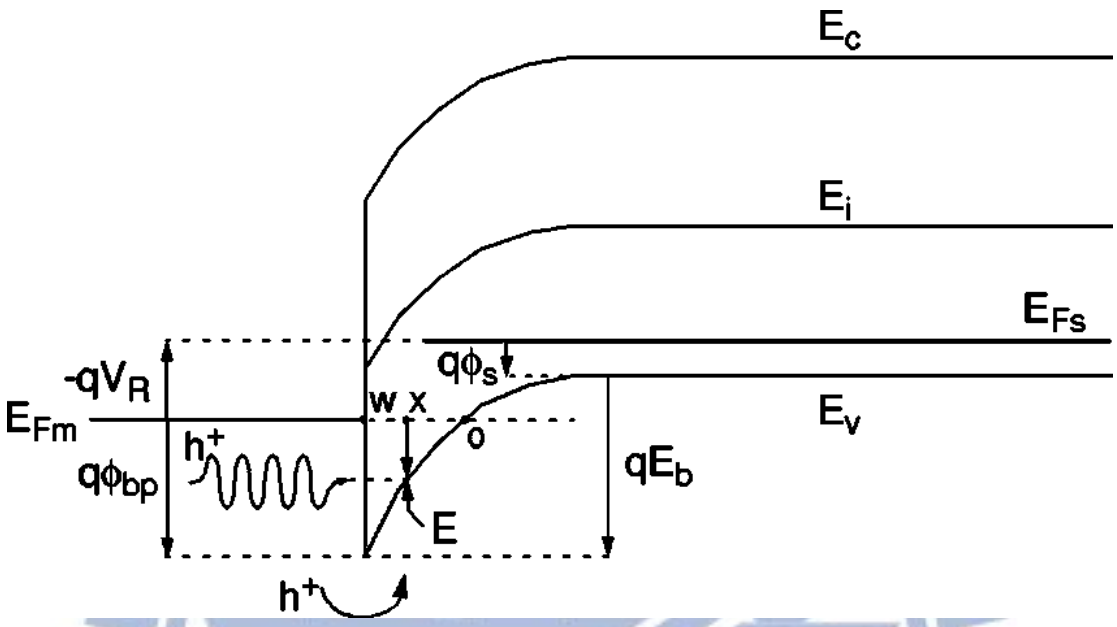

Fig.2-1 Thermionic-field emission schematic diagram. Holes in the metal are thermally activated and penetrating the Schottky barrier.

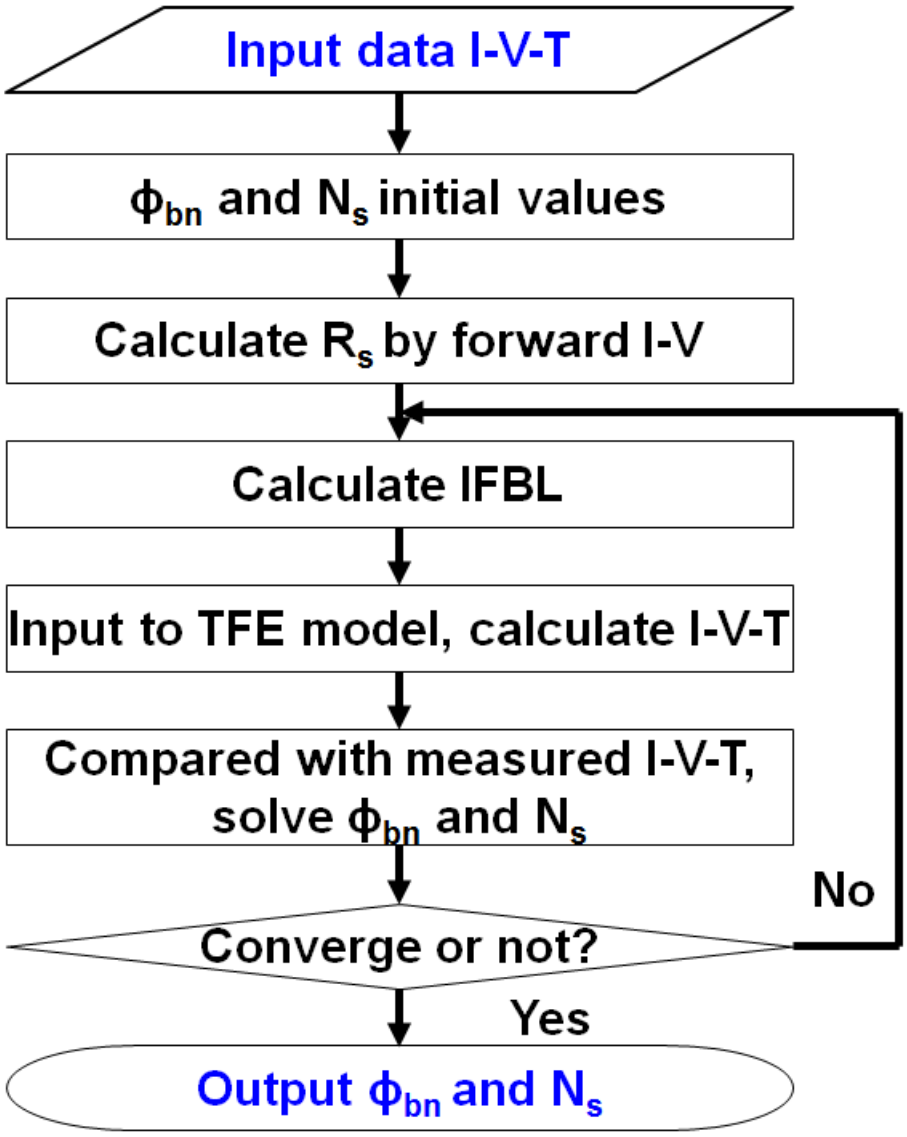

Fig.2-2 Extraction flow of TFE method. This procedure is realized by the math tool MATLAB.

(a)

(b)

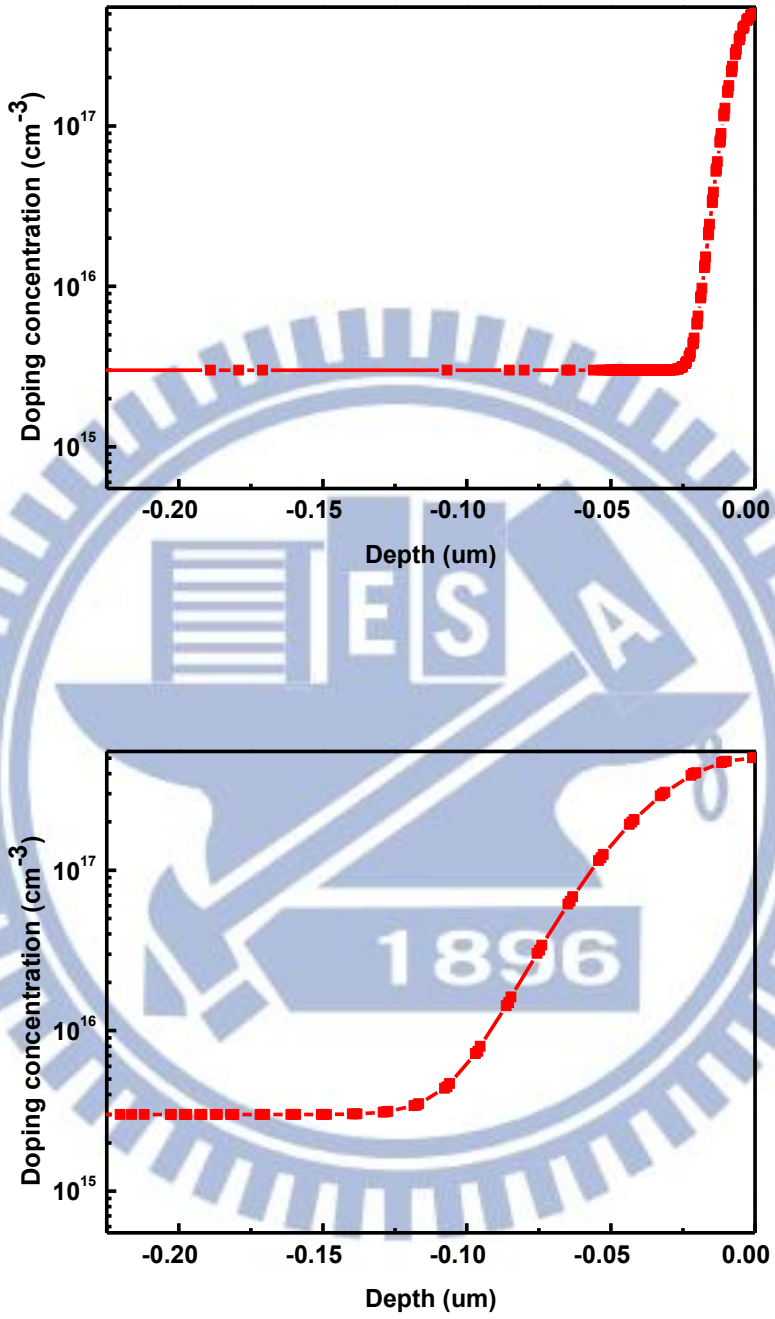

Fig.2-3 Gaussian doped profiles of the simulation. (a) The peak concentration is set to 5×10^{17} cm^{-3}, and the depth of the profile is set to 20 nm (b) The peak concentration is set to 5×10^{17} cm^{-3}, and the depth of the profile is set to 100 nm

(a)

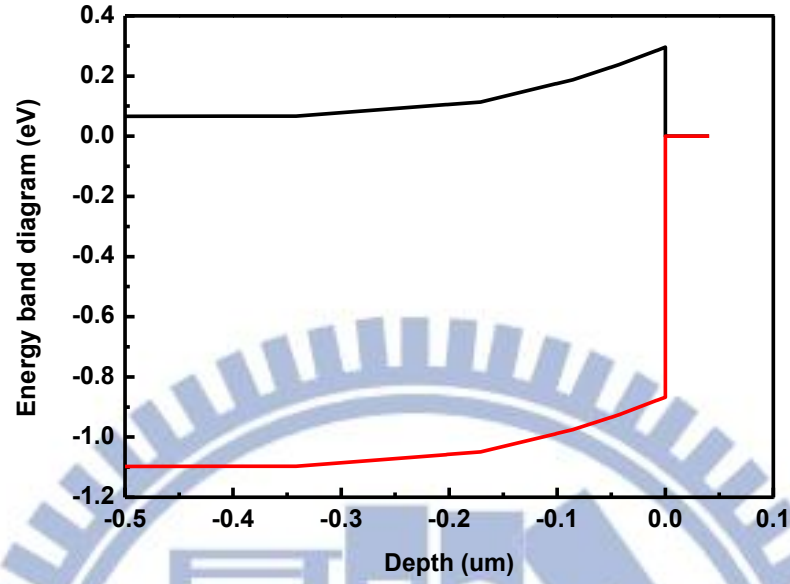
Energy band diagram (eV)
0.4
0.2
0.0
-0.2
-0.4
-0.6
-0.8
-1.0
-1.2
-0.5
-0.4
-0.3
-0.2
-0.1
0.0
0.1
Depth (um)

(b)

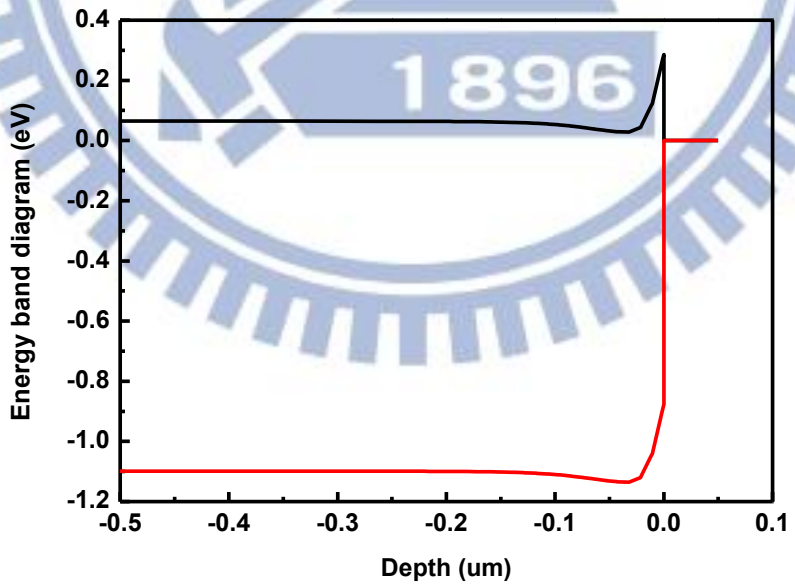
Energy band diagram (eV)
0.4
0.2
0.0
-0.2
-0.4
-0.6
-0.8
-1.0
-1.2
-0.5
-0.4
-0.3
-0.2
-0.1
0.0
0.1
Depth (um)

(c)

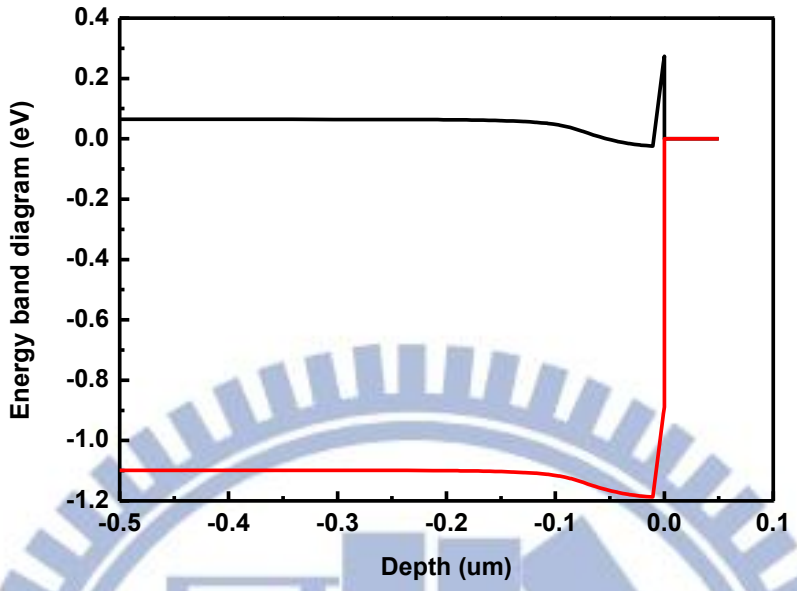
Energy band diagram (eV)
0.4
0.2
0.0
-0.2
-0.4
-0.6
-0.8
-1.0
-1.2
-0.5
-0.4
-0.3
-0.2
-0.1
0.0
0.1
Depth (um)

(d)

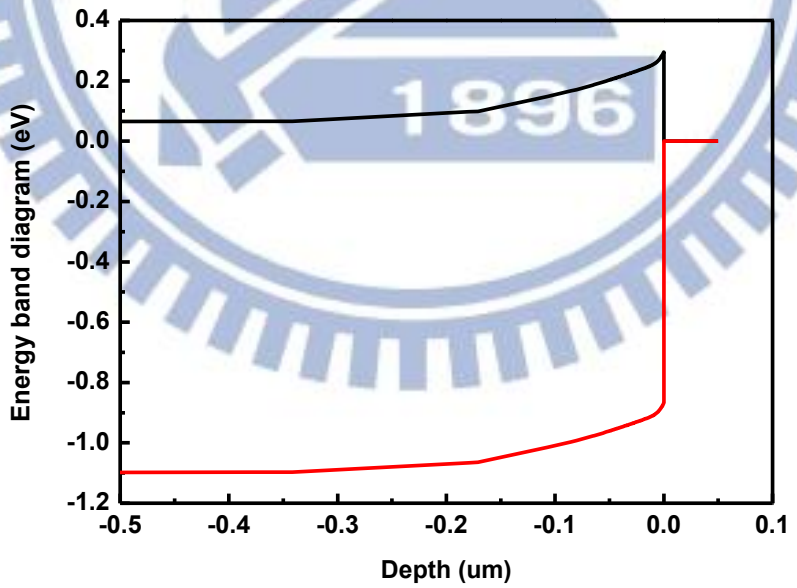
Energy band diagram (eV)
0.4
0.2
0.0
-0.2
-0.4
-0.6
-0.8
-1.0
-1.2
-0.5
-0.4
-0.3
-0.2
-0.1
0.0
0.1
Depth (um)

(e)

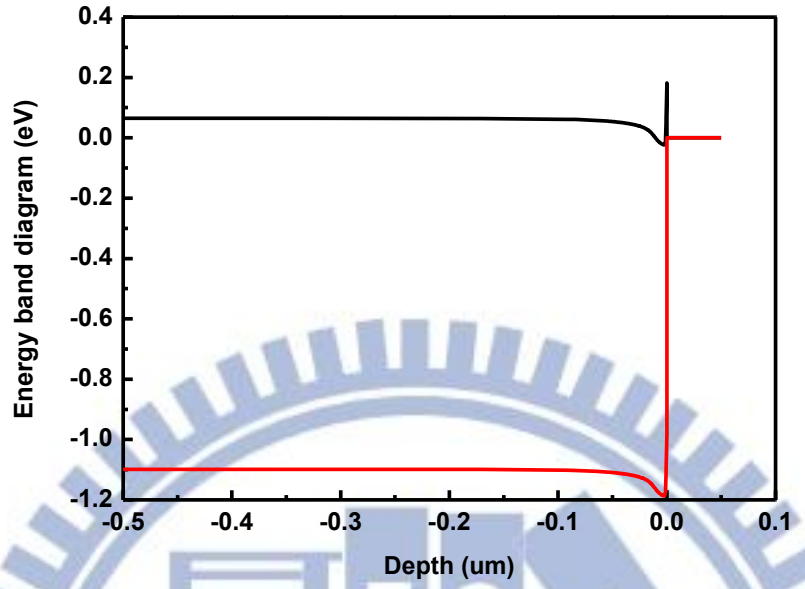

Fig.2-4 Energy band diagrams of the simulation. (a) Constant doping profile, the substrate doping concentration is set to 3×10^{15} cm^{-3} (b) Gaussian doped profile, the substrate doping concentration is set to 3×10^{15} cm^{-3}, peak concentration is 5×10^{17} cm^{-3}, and the depth is 100 nm (c) Gaussian doped profile, the substrate doping concentration is set to 3×10^{15} cm^{-3}, peak concentration is 1×10^{20} cm^{-3}, and the depth is 100 nm (d) Gaussian doped profile, and the substrate doping concentration is set to 3×10^{15} cm^{-3}, peak concentration is 5×10^{17} cm^{-3}, and the depth is 20 nm (e) Gaussian doped profile, and the substrate doping concentration is set to 3×10^{15} cm^{-3}, peak concentration is 1×10^{20} cm^{-3}, and the depth is 20 nm

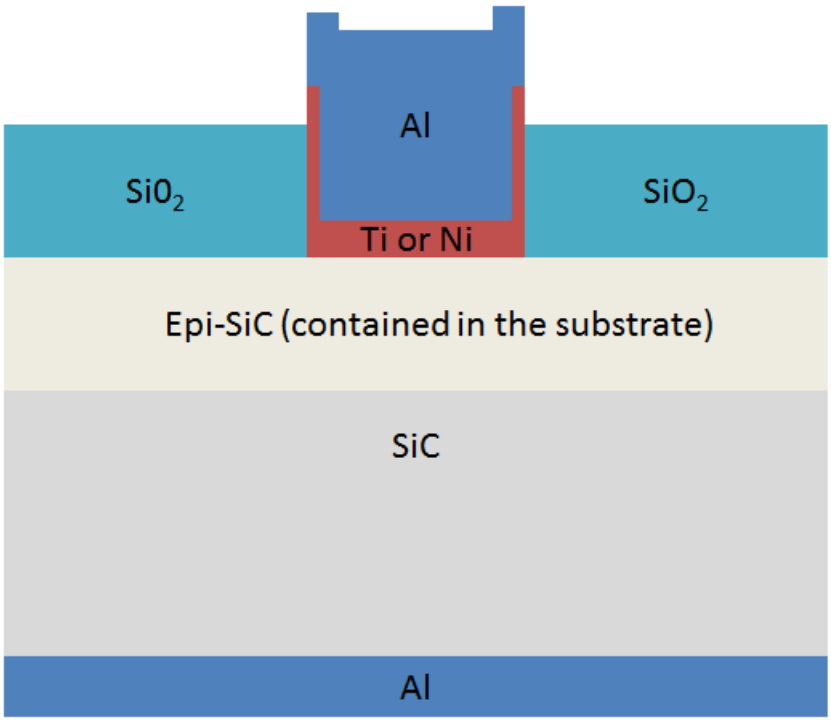

Fig.2-5 Device configuration of Metal/SiC Schottky junction.

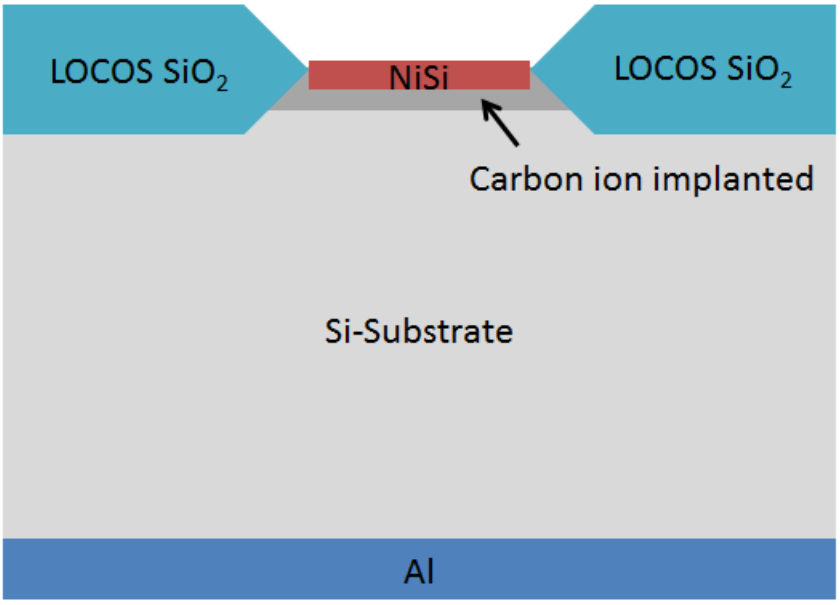

Fig.2-6 Device configuration of Metal/Si Schottky junction with carbon ion implantation.

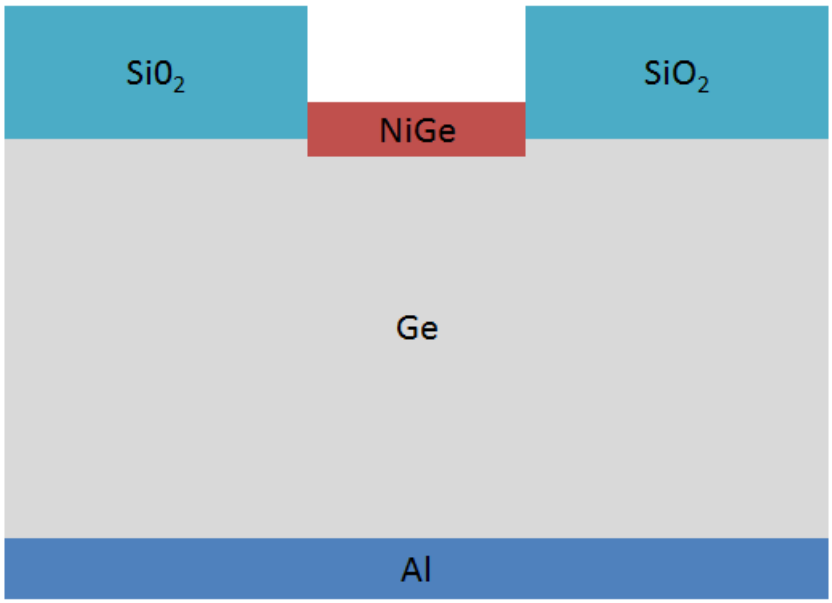

Fig.2-7 Device configuration of Metal/Ge Schottky junction.

(a)

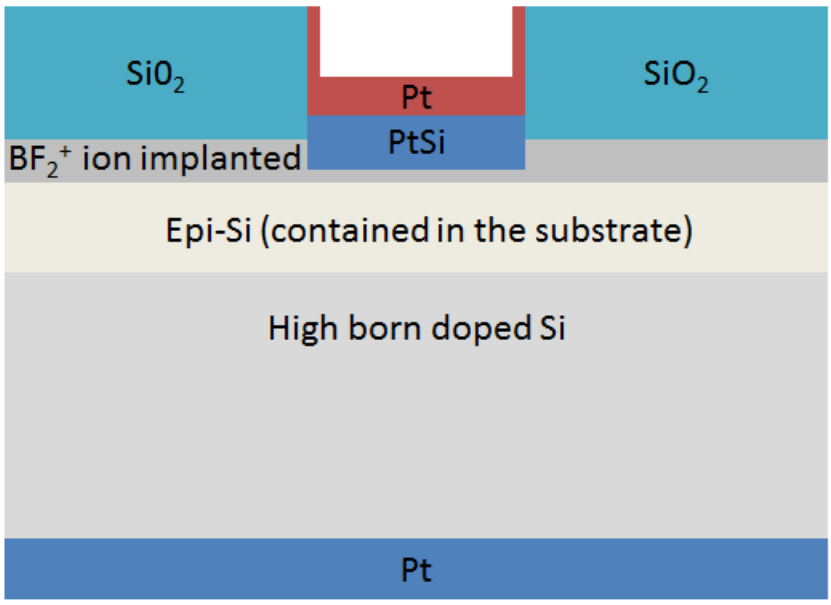

(b)

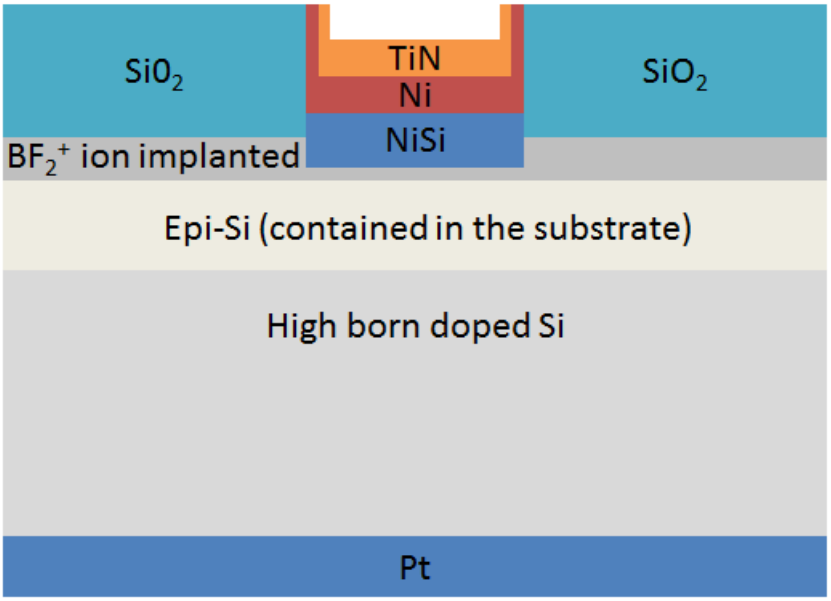

Fig.2-8 Device configurations of Metal/p-Si Schottky junction with BF_2^+ ion implantation (a) PtSi/p-Si (b) NiSi/p-Si

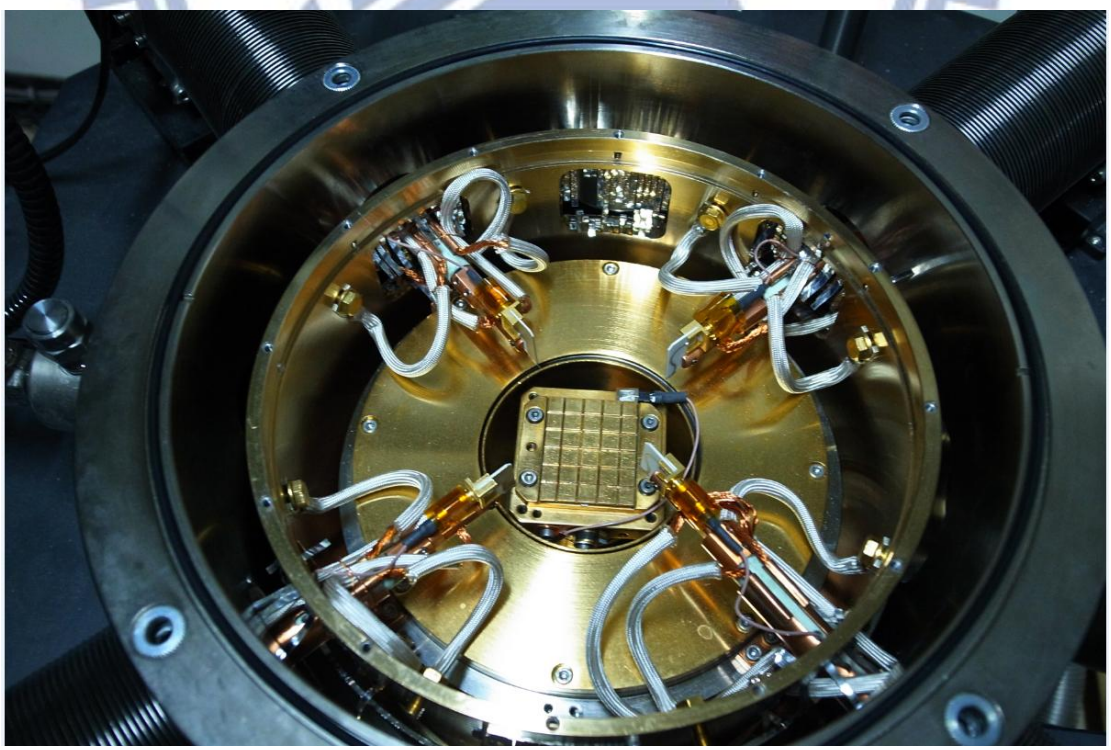

Fig.2-9 The chamber of the probe station Lake Shore CPX-VF

Chapter 3

Simulation Results and Discussion

3-1 Schottky Barriers with Constant Doping Profile

To evaluate if accurate Schottky barrier height (SBH) can be extracted by the proposed extraction procedure, TCAD tool is used to generate the I-V-T characteristics of Schottky junctions with various SBH and substrate doping profiles. Then, the SBH and surface doping concentration (N) are extracted from the simulated I-V-T characteristics using the proposed extraction procedure. At forward bias, the SBH and the ideality factor (n) are extracted by the TE model while at reverse bias; the SBH and N are extracted by the TFE model. At last, comparison between the extracted parameters and the preset parameters in the TCAD simulation are performed.

Fig.3-1 shows the electrical characteristics of the Schottky junction with a metal work function of 4.55 eV. According to the concept of ideal Schottky barrier formation, the SBH here is 0.5 eV. The electrical characteristic at temperature of 100 K is incorrect because the current at reverse bias is too small to be simulated due to the convergence problem of the Schottky-Read-Hall model in the TCAD tool. For the medium SBH, the SBH can be extracted either from the forward biased I-V characteristic using the TE model or from the reverse biased I-V characteristic using the TFE model. The parameters extracted by the TE and TFE models are shown in Table 3-1 and 3-2, respectively. The extracted results from the TE model show that the barrier heights at different temperatures are very close to 0.5 eV, and it means that the TCAD simulation is correct. However, the ideality factor at temperature of 300 K is

not precise enough because the extraction method by the TE model is based on the linear region in the log(I)-V plot at forward bias, and the linear region is too small to extract the parameters precisely at this temperature.

3-1.1 Difference between Simulation and Extraction Model

After confirming the validity of the simulation, the extracted results from the TFE model are listed in Table 3-2. Before discussing the results from TFE model, two parameters in this model need to be classified. BH0 is the barrier height ignoring the IFBL effect, and BH is the barrier height considering the IFBL effect at zero bias. The extracted result at 100 K is not shown because the simulated reverse conducting current at this temperature is invalid. For the ideal Schottky barrier, the extracted BH0 should be close to the preset value, i.e. 0.5 eV. However, the extracted results show that the BHs are much closer to 0.5 eV than the BH0s because the IFBL model in the TCAD tool is too simple to reflect the barrier height at the bias of 0 V. The simplified IFBL model in the TCAD tool is expressed as

$$\Delta\phi_b = 2.6\times10^{-4}\times\left(\left(\frac{E}{E_0}\right)^{p1}-\left(\frac{E_{eq}}{E_0}\right)^{p1}\right),$$

where E_{eq} is the electric field at the bias of 0 V, and the others are fitting parameters for different materials. In other words, the simulated electrical characteristics near the bias of 0 V show less IFBL effect, but in reality this effect still exists. This is the reason why the BHs are much closer to the preset value than the BH0s. Because the doping concentration in logarithm scale is more sensitive to the conducting current, the extracted doping concentration could be viewed close enough to the preset value. In the case of the barrier height of 0.5 eV, extracted results from either TE model or TFE model are all consistent with the preset values.

For comparing the real IFBL effects with the TCAD tool in detail, the characteristic differences are shown in Fig.3-2. The reverse biased I-V characteristic depends on the IFBL effect strongly, the larger amount of the IFBL effect the higher order of the leakage current. By observing the leakage current in Fig.3-2, the IFBL effect as a function of voltage bias can be estimated. It is known that there is no IFBL effect at zero bias in the TCAD tool, so the current order near the zero bias is lower than that in the extraction model: the actual SBH at zero bias is lower than 0.5 eV after taking the real IFBL effect into consideration, so the current magnitude is higher in real case. With higher voltage drop the amount of the IFBL effects in both two models becomes evident, because the current magnitudes of these two models rise higher. However, the rising speed of the TCAD simulated result is much faster than that of the theoretical calculated result. The IFBL effect in the TCAD tool is too simple, so the dependence on the voltage drop must be strong enough in order to fit the real cases. At the bias of about -1.8 V the amounts of the IFBL effect in these two models seem to be equal, and it means that the IFBL effect in the TCAD tool will be stronger after this bias.

3-1.2 The Temperature Limits of Extraction Models

In order to observe the temperature limits of these two extraction methods, the SBH is lowered to 0.3 eV by setting the metal work function to 4.35 eV. The simulated electrical characteristics are shown in Fig.3-3. Fig.3-4 and Table 3-3 show the extracted results from the TE model. The results are consistent with the preset values. Apparently, the electrical characteristics at temperatures higher than 200 K cannot be used for extracting the SBH by the TE model, because the linear region at forward bias disappears. The conducting current at forward bias is severely suffered

from the parasitic resistance at high temperature, so the Schottky barrier plays minor role.

Following are discussion on the extracted results from the TFE model. The available results shown in Table 3-4 are also consistent with the preset values. The TFE model works at high temperature, because this model utilizes the conducting current at reverse bias. The Schottky barrier has higher impedance than the parasitic resistance at reverse bias, so the conducting current is dominant by the Schottky barrier. But there is still a temperature limit for the TFE model; the extracted result at temperature of 300 K is unavailable, because the simulated characteristic is dominated by parasitic resistance purely. In the extraction procedure using the TFE model, all the voltage drops due to the parasitic resistance have been deducted, so the I-V characteristic does not provide sufficient information for extracting the SBH.

3-1.3 Effects of the Doping Concentrations

Before studying the effects of the non-uniform doping profile, there is one more thing needed to be studied. The extraction method by the TFE model we proposed here is derived on the basis of constant doping profile, so the barrier height extraction by this method on the non-uniform doped substrate should be careful. In order to observe how to obtain correct results and how to explain the extracted results, it is necessary to study the conducting current of the TFE model at reverse bias with different doping profiles. Fig.3-5 shows the electrical characteristics of the TFE model calculated by MATLAB, and these calculations does not consider the parasitic resistance. To avoid the mesh generation and the effective IFBL model problems in the TCAD tool, the calculation of the uniform doped Schottky junction characteristics by MATLAB are much easier and more correct, but such a method is hard for

non-uniform doped cases. There are two phenomena should be emphasized: one is the slope of the current density in logarithm scale would be larger as the doping concentration raises, and the other is the current density close to the bias of 0 V is larger as the doping concentration is higher. However, how to obtain the correct results will be introduced later.

3-2. Schottky Barriers with Gaussian Doped Profile

In order to observe the effect of ion implantation in real devices, the I-V characteristics of Schottky barriers with various Gaussian doping profiles are studied here. In most cases, the barrier height is set to 0.3 eV and the background doping is set to 3×10^{15} cm^{-3}. We replace the doping profile near the Schottky junction with a Gaussian profile. There are two new variables need to be defined. One is the junction depth which decides how deep the doping concentration lowers to the substrate doping concentration, and the other is the peak concentration of the Gaussian doping profile. The temperature of the simulation only ranges from 100 K to 200 K, because the current at the temperature higher than 200 K is dominated by parasitic resistance even at reverse bias.

3-2.1 Effects of the Peak Concentration

Fig.3-6, Fig.3-7, Fig3-10 and Fig.3-11 show the simulated electrical characteristics of the Schottky barriers with different Gaussian doping profiles. First, we study the cases of junction depth set to 100 nm with the peak concentration of $5x10^{17}$ and $1x10^{20}$ cm^{-3} as shown in Fig.3-6 and Fig.3-7, respectively. After comparing these two figures with Fig.3-3, some differences could be observed at reverse bias. The slopes of the J-V curves have been larger near the bias of 0 V,

Fig.3-6 shows that the slopes raise at first but soon lower down after the bias of -0.5 V, and it means that the doping region of the 100-nm-deep Gaussian doping profiles has been fully depleted by the reverse bias. However, Fig.3-7 shows that the doping region of the Gaussian doping profiles would not be fully depleted even at higher bias as the peak doping concentration increases to $1x10^{20}$ cm^{-3}. In this case, the current density becomes dominated by parasitic resistance at high voltage and high temperature.

From the study of section 3-1.3 we know that the slopes of the J-V curves at reverse bias would respond to the doping concentration. In the case of Fig.3-6, the data after the bias of -0.5 V are all neglected in the extraction procedure of the TFE model, because they respond to the substrate doping but not the Gaussian doping near the Schottky junction. After neglecting these data, the SBH extracted by the TFE model would be more precise, but the extracted doping concentration would be the effective value in the Gaussian doping region.

First, the extractions of the case with junction depth set to 100 nm and peak concentration set to 5×10^{17} cm^{-3} are studied. The energy band diagram has been shown in Fig.2-4(b), and the width of the barrier becomes shorter than that with constant doping profile. The extracted results by the TE model are listed in Table 3-5 and Fig.3-8, and the results are consistent with the preset values. However, the ideality factor is a little away from the theoretical value of 1 because the doping concentration would be the variable caused the ideality factor raised [51]. The extracted results by the TFE model are listed in Table 3-6 and Fig.3-8. The barrier heights are consistent with the preset value of 0.3 eV, and the extracted doping concentrations are a bit lower than the preset value of 5×10^{17} cm^{-3}.

Next, the extracted results of the case with junction depth set to 100 nm and peak concentration set to 1×10^{20} cm^{-3} are studied. As the peak concentration increases to

$1x10^{20}$ cm^{-3}, the band diagram is shown in Fig.2-4(c), and the width of the barrier becomes even shorter than that in the case of the peak concentration of 5×10^{17} cm^{-3}. The extracted results by the TE model are listed in Table 3-7 and Fig.3-9, and the results are not consistent with the preset values anymore. The extracted barrier heights are a bit lower than the preset value of 0.3 eV, and the extracted ideality factors are larger than those listed in Table 3-5. It is clear that the extraction of barrier height by the TE model starts to be unreliable. The extracted results by the TFE model are listed in Table 3-8 and Fig.3-9. The extracted barrier heights are still consistent with the preset value of 0.3 eV, but the extracted doping concentrations are far lower than the preset peak value of 1×10^{20} cm^{-3}. Comparing to the doping concentrations listed in Table 3-6 and Fig.3-y, these results are a bit higher as expected.

3-2.2 Effects of the Junction Depth

In this subsection, the junction depth is shortened to 20 nm to study the effect of the depth of the non-uniform doping region. The electrical characteristics are shown in Fig.3-10 and Fig.3-11. The simulated I-V characteristics are compared at first. Apparently, the region with high slope cannot be observed anymore, but the magnitude of the current density is higher than that in the case of constant doping profile. It also means that it is hard to extract correct results by the TFE model.

The band diagram of the case with junction depth set to 20 nm and peak concentration set to 5×10^{17} cm^{-3} has been shown in Fig.2-4(d). The extracted results by the TE model are listed in Table 3-9 and Fig.3-12. The barrier heights are a bit lower than the preset value of 0.3 eV, and the ideality factors are a bit larger than the ideal value of 1 expectedly. The extracted results by the TFE model are listed in Table 3-10 and Fig.3-12, and the extracted barrier heights are not consistent with the preset

value. The results of doping concentration are lowered to the order of the substrate doping because the 20-nm-deep non-uniform doping layer is depleted completely by the Schottky barrier.

The electrical characteristics of the case with junction depth set to 20 nm and peak concentration set to 1×10^{20} cm^{-3} are shown in Fig.3-11. It is apparent that the electrical characteristics are all dominated by parasitic resistance, so the extraction methods by either TE model or TFE model cannot be used anymore. It might be caused by the high electric field near the Schottky junction, which can be observed in Fig.2-4(e). The barrier is too thin to avoid tunneling of the electron at reverse bias, and electrons can easily flow into the semiconductor even at very low temperature [51].

3-3 Summary

In the cases of constant doped profiles, the simulated result shows that the TE model is not suitable for extracting the SBH. As the SBH lowering or the measuring temperature increasing, the impedance on the SB would be smaller than that on the parasitic resistance, so the conducting mechanism would not be dominated by the TE model but by the parasitic resistance. However, the TFE model utilizes the conducting mechanism at reverse bias, so such a method could be adopted in higher temperature region and lower SBH cases. For example of 0.3 eV cases, the suitable temperature region is up to 250 K for the TFE model, and it has a promotion of 100 K in comparison with the TE model.

In the cases of Gaussian doped profiles, the simulated result shows that the suitable temperature region for the TE model has been much shorten due to the increasing of N. In the cases of deeper Schottky junctions, e.g. junction depth is 100

nm, the Gaussian doped region would not be fully depleted at zero bias, so the effect of the reverse bias on the Gaussian doped region could be measured. The extracted result from the TE model shows that the SBH would be effectively lowered due to the IFBL effect. For the peak concentration of 5×10^{17} cm^{-3}, the effectively lowering amount is about 0.01 eV, and it would be raised to 0.02 eV for the peak concentration of 1×10^{20} cm^{-3}. However, the TFE model has the ability to separate the IFBL effect from the real SBH, so we could extract the SBH more accurately. For the TFE model, the extracted SBHs would be much closer to the preset value, but the extracted N would be an effective value for the Gaussian doped region.

In the cases of shallower Schottky junctions, e.g. junction depth is 20 nm, the Gaussian doped region may be fully depleted even at zero bias for low peak concentration. The effect of the reverse bias on the Gaussian doped region could not be measured, so the TFE model loses the ability to separate the IFBL effect from the real SBH, and the effectively lowering amount is about 0.027 eV for both the TE model and the TFE model. However, the Gaussian doped region would not be fully depleted at zero bias for high peak concentration, but the high electrical field results in the disappearing of the rectifying effect even at low temperature. The SBH could be extracted by neither TE model nor TFE model due to the electrical characteristic of purely parasitic resistance.

Table 3-1 Traditional TE extraction result of barrier height set to 0.5 eV with constant doping profile.

TE	100 K	150 K	200 K	250 K	300 K
BH (eV)	0.498	0.502	0.505	0.508	0.509
N	1.01	1.01	1.03	1.02	1.48

Table 3-2 TFE extraction result of barrier height set to 0.5 eV with constant doping profile.

TFE	100 K	150 K	200 K	250 K	300 K
BH0 (eV)	NA	0.515	0.510	0.510	0.511
BH (eV)	NA	0.499	0.498	0.497	0.496
N (10^{15} cm^{-3})	NA	3.25	2.17	2.79	3.96

Table 3-3 Traditional TE extraction result of barrier height set to 0.3 eV with constant doping profile.

TE	100 K	150 K	200 K	250 K	300 K
BH (eV)	0.299	0.303	NA	NA	NA
n	1.02	1.01	NA	NA	NA

Table 3-4 TFE extraction result of barrier height set to 0.3 eV with constant doping profile.

TFE	100 K	150 K	200 K	250 K	300 K
BH0 (eV)	0.309	0.305	0.305	0.305	NA
BH (eV)	0.297	0.299	0.298	0.297	NA
N (10^{15} cm^{-3})	2.08	2.13	2.38	1.85	NA

Table 3-5 Traditional TE extraction result of barrier height set to 0.3 eV with Gaussian doping profile of junction depth set to 100 nm and peak concentration set to 5×10^{17} cm^{-3}.

TE	100 K	150 K	200 K
BH (eV)	0.293	0.288	NA
n	1.06	1.19	NA

Table 3-6 TFE extraction result of barrier height set to 0.3 eV with Gaussian doping profile of junction depth set to 100 nm and peak concentration set to 5×10^{17} cm^{-3}.

TFE	100 K	150 K	200 K
BH0 (eV)	0.329	0.336	0.338
BH (eV)	0.295	0.292	0.293
N (10^{17} cm^{-3})	1.17	2.12	1.41

Table 3-7 Traditional TE extraction result of barrier height set to 0.3 eV with Gaussian doping profile of junction depth set to 100 nm and peak concentration set to 1×10^{20} cm^{-3}.

TE	100 K	150 K	200 K
BH (eV)	0.277	0.277	NA
n	1.25	1.32	NA

Table 3-8 TFE extraction result of barrier height set to 0.3 eV with Gaussian doping profile of junction depth set to 100 nm and peak concentration set to 1×10^{20} cm^{-3}.

TFE	100 K	150 K	200 K
BH0 (eV)	0.345	0.346	0.353
BH (eV)	0.300	0.291	0.295
N (10^{18} cm^{-3})	3.32	7.66	7.03

Table 3-9 Traditional TE extraction result of barrier height set to 0.3 eV with Gaussian doping profile of junction depth set to 20 nm and peak concentration set to 5×10^{17} cm^{-3}.

TE	100 K	150 K	200 K
BH (eV)	0.276	0.272	NA
n	1.03	1.21	NA

Table 3-10 TFE extraction result of barrier height set to 0.3 eV with Gaussian doping profile of junction depth set to 20 nm and peak concentration set to 5×10^{17} cm^{-3}.

TFE	100 K	150 K	200 K
BH0 (eV)	0.284	0.285	0.285
BH (eV)	0.273	0.273	0.272
N (10^{15} cm^{-3})	1.36	2.62	4.75

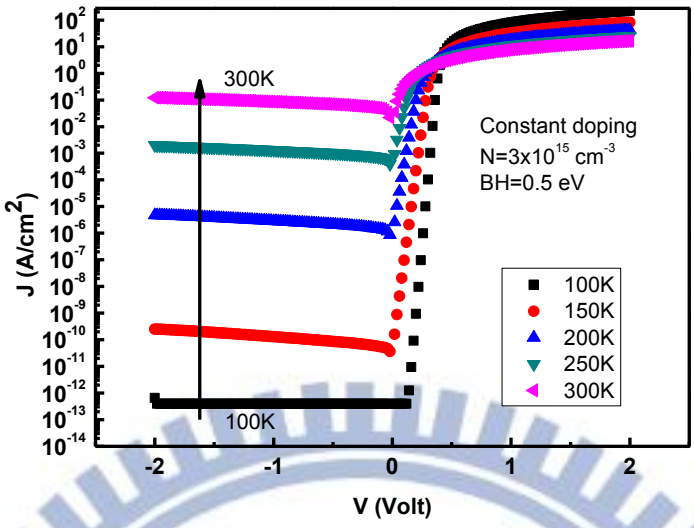

Fig.3-1 Electrical characteristics are simulated by Sentaurus with constant doping profile and metal work function set to 4.55 eV. Temperature ranges from 100 to 300 K.

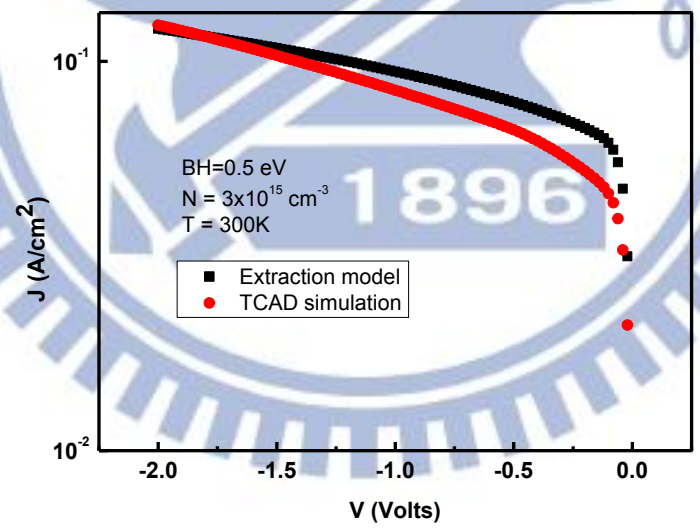

Fig.3-2 Characteristics difference at the temperature of 300 K between the TFE model and the TCAD tool. The SBH is set to 0.5 eV, and the doping concentration is set to $3x10^{15}$ cm^{-3}.

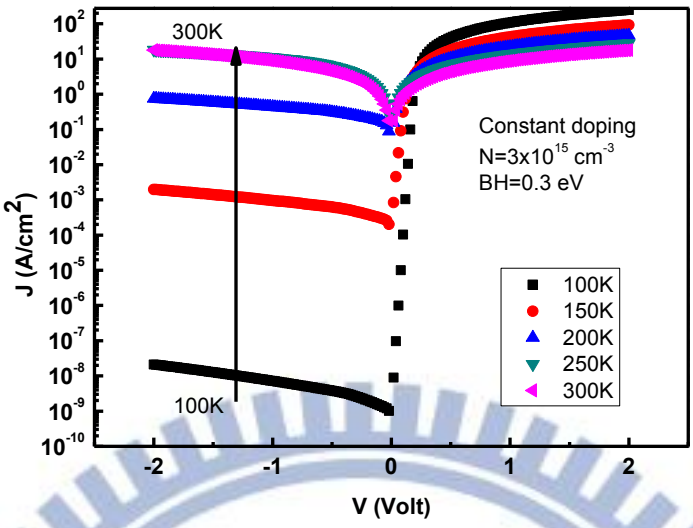

Fig.3-3 Electrical characteristics are simulated by Sentaurus with constant doping profile and metal work function set to 4.35 eV. Temperature ranges from 100 to 300 K.

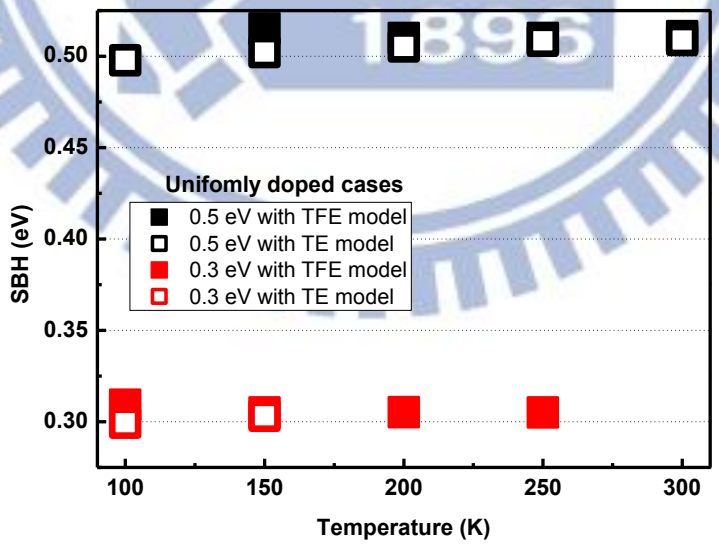

Fig.3-4 Extracted SBHs with TE model and TFE model for uniformly doped cases.

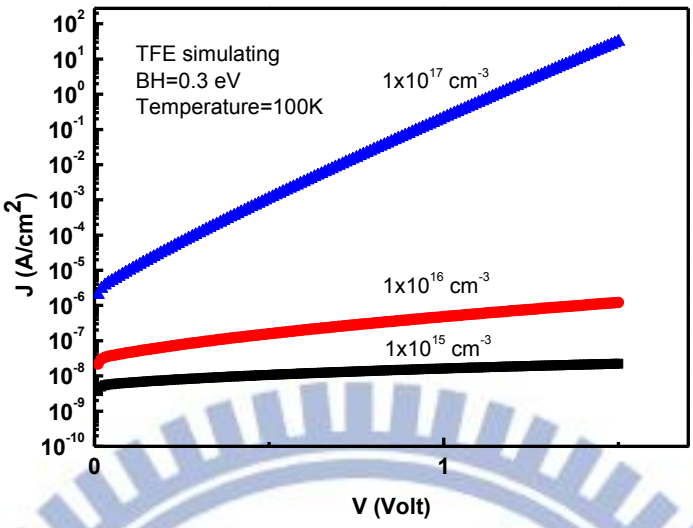

Fig.3-5 Electrical characteristics are simulated by MATLAB with TFE model. The barrier height is set to 0.3 eV and the temperature is set to 100 K. Doping concentration ranges from 1×10^{15} to 1×10^{17} cm^{-3}.

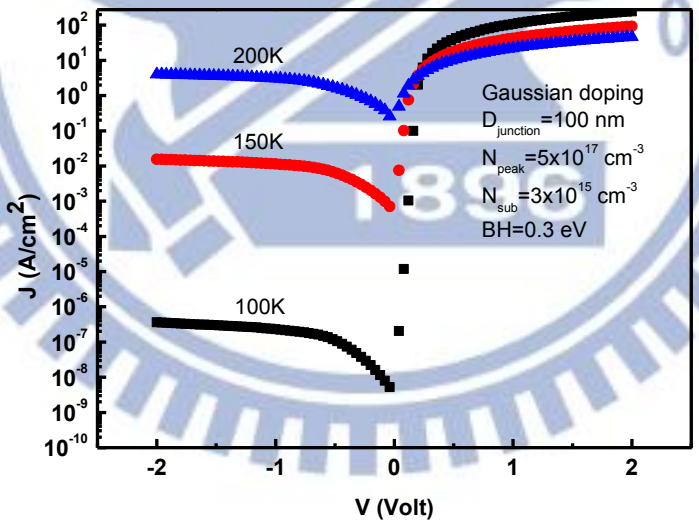

Fig.3-6 Electrical characteristics are simulated by Sentaurus with Gaussian doping profile and metal work function set to 4.35 eV. The junction depth of Gaussian profile is set to 100 nm and the peak concentration is set to 5×10^{17} cm^{-3}. Temperature ranges from 100 to 200 K.

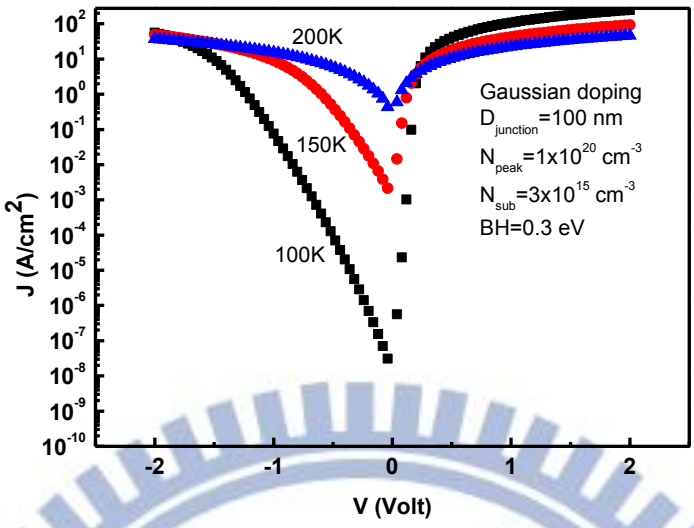

Fig.3-7 Electrical characteristics are simulated by Sentaurus with Gaussian doping profile and metal work function set to 4.35 eV. The junction depth of Gaussian profile is set to 100 nm and the peak concentration is set to 1×10^{20} cm^{-3}. Temperature ranges from 100 to 200 K.

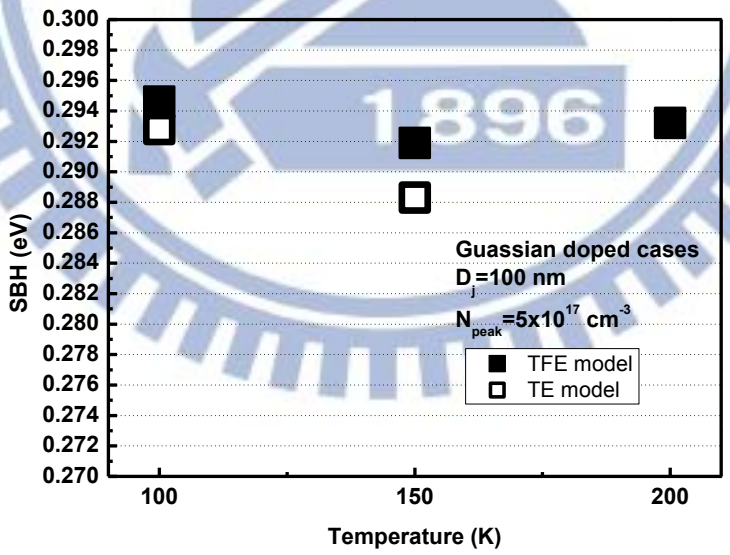

Fig.3-8 Extracted SBHs with TE model and TFE model for Gaussian doped case. The junction depth is set to 100 nm and the peak concentration is set to 5×10^{17} cm^{-3}.

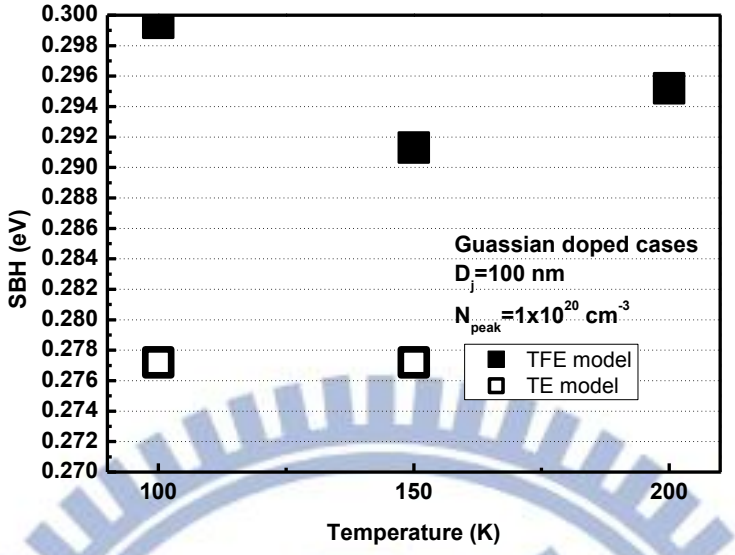

Fig.3-9 Extracted SBHs with TE model and TFE model for Gaussian doped case. The junction depth is set to 100 nm and the peak concentration is set to 1×10^{20} cm^{-3}.

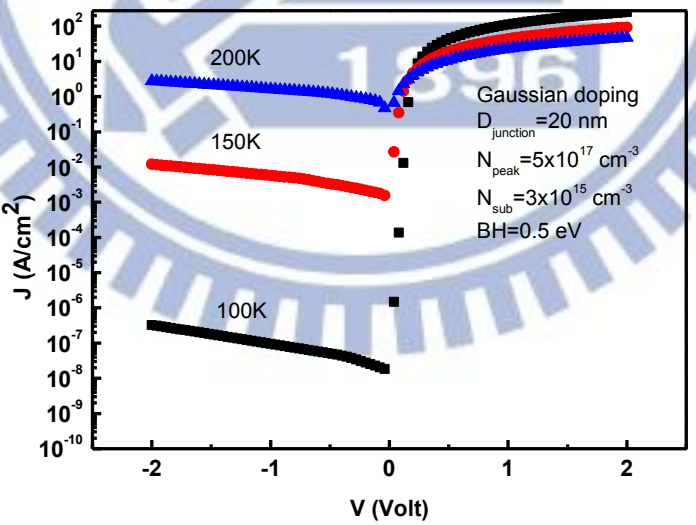

Fig.3-10 Electrical characteristics are simulated by Sentaurus with Gaussian doping profile and metal work function set to 4.35 eV. The junction depth of Gaussian profile is set to 20 nm and the peak concentration is set to 5×10^{17} cm^{-3}. Temperature ranges from 100 to 200 K.

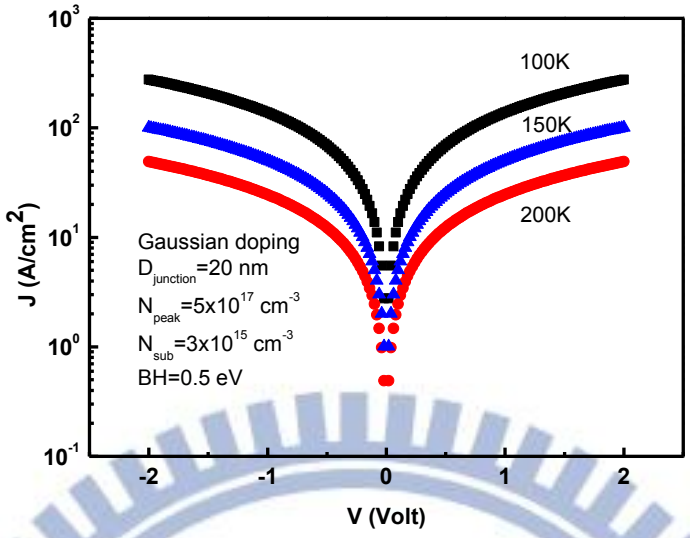

Fig.3-11 Electrical characteristics are simulated by Sentaurus with Gaussian doping profile and metal work function set to 4.35 eV. The junction depth of Gaussian profile is set to 20 nm and the peak concentration is set to 1×10^{20} cm^{-3}. Temperature ranges from 100 to 200 K.

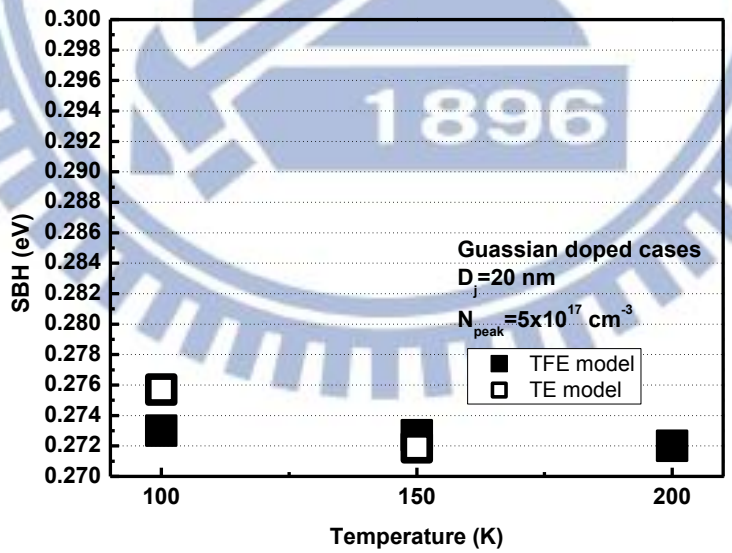

Fig.3-12 Extracted SBHs with TE model and TFE model for Gaussian doped case. The junction depth is set to 20 nm and the peak concentration is set to 5×10^{17} cm^{-3}.

Chapter 4

Experiment Results and Discussion

4-1 Medium and High Height Extractions

The SBH extraction procedure has been verified by simulations in Chapter 3, including the cases of constant and Gaussian doping profiles. The simulations provide good references for the experiment cases, so the effects caused by the different fabrication processes could be explained. The case of constant doping profile is simulated for the Schottky junction on uniform doped substrate, and the case of Gaussian doping profile is simulated for the Schottky junction on ion implanted substrate. In order to ensure that the extraction procedure proposed in Chapter 2 could be adopted in real Schottky junctions, the procedure is verified again by the Metal/n-SiC Schottky junctions in this section. Afterwards, the effect of carbon ion implantation on NiSi/n-Si Schottky junction is studied.

4-1 .1 Metal/n-SiC Schottky Junctions

SiC is a potential semiconductor material for high-power, high-temperature and high-frequency devices for applications in aerospace and ground-based power system. Due to the higher breakdown electric field and wider band gap of SiC, high-voltage Schottky diodes with relatively lower leakage current and on-resistance compared to Si Schottky diodes can be fabricated on SiC. Both Ti/ and Ni/n-SiC Schottky junctions are studied here.

First, the electrical characteristics of Ni/n-SiC Schottky junction and the extraction results are shown in Fig.4-1. In this case, the conducting current at reverse

bias is too low to be measured at room temperature, so the temperatures of the measurement were raised to 423 K and 448 K. The extraction results of both TE model (at forward bias) and TFE model (at reverse bias) are consistent with those reported in literatures [52-53], and the extracted BH0 is about 1.42 eV at both temperatures. It means the SBH without IFBL model is caused by Fermi-level pinning, but the SBH with IFBL model would be differed from the temperatures. The amount of IFBL depends on the energy band bending, and the amount of the band bending at 423 K is a bit larger than that at 448 K, because the conduction band edge would be away from Fermi-level at higher temperature. The amount of IFBL at 423 K is a bit larger than the amount at 448 K, so the SBH at 423 K is lower. Second, the electrical characteristics of the Ti/n-SiC Schottky junction and the extraction results are shown in Fig.4-2, and the temperature of measurement was at 300 K. The extraction results by both TE and TFE models are also consistent with those reported in literatures [32, 54].

Both two cases of Ni and Ti/n-SiC Schottky junctions are successfully extracted by the procedure proposed in Chapter 2, and this means the procedure could be adopted in real case. However, the SBHs on SiC extracted here are still far from the goal of exact low SBH extraction, so following is the Schottky junction on Si.

4-1 .2 Effect of Carbon Ion Implantation

Schottky barrier S/D-MOSFETs have been widely investigated as a promising candidate in sub-30 nm CMOS technology nodes [55]. Due to the low resistivity, low Si consumption, and low process temperature, NiSi is the most frequently studied metal silicide in SB-MOSFETs. However, the work function of NiSi lies close to the middle of the Si energy band gap, so the large SBH to both n- and p-type Si degrades

the drive current. In order to adjust the SBH, carbon ion implantation has been studied, but most literature only gives effective results of the SBH [56]. In this part, effects of carbon ion implantation to Schottky junction is studied, including how it affects SBH and doping concentration.

In order to ensure that the conducting mechanism at reverse bias in this case is still dominated by TFE model, the electrical characteristics are measured at different temperatures, ranges from 300 K to 350 K, as shown in Fig.4-3. The electrical characteristics are consistent with the dependence of temperatures, the higher temperature the higher leakage current. Furthermore, the leakage current here shows one significant phenomenon: the slope of the J-V characteristics rises rapidly at first, and then lowers down. This phenomenon is consistent with the simulated characteristics with Gaussian doped profile, so the assumption is made: the effect of carbon ion implantation is contributing more electrons as what dopants work. The SBHs are extracted by both TE and TFE models and the results of SBH, ranges from 0.57 to 0.59 eV. It means that the conducting current in this case is still dominated by Schottky junction and the SBH without IFBL (BH0) model is 0.65 eV. The SBH without IFBL model is consistent with the value of NiSi/n-Si Schottky junction reported in literature [17], but the exact SBH is lowered to about 0.58 eV.

The extracted doping concentration here raises to about 10^{18} cm^{-3}. This high concentration results in significant IFBL effect, and this is the reason why the extracted SBH is lowered down. The amount of IFBL highly depends on the doping concentration, and the temperature dependence of the SBH is more obvious than that in the case of SiC Schottky junction studied previously. In order to ensure that the electrons are increased by carbon ion implantation, the SIMS and SRP depth profiles before silicide formation are shown in Fig.4-4. The concentration of carbon near the Schottky junction, about 30 nm below the original Si surface, is about 10^{20} cm^{-3}.

However, SRP measurement shows the activated electron concentration near the junction is only about 10^{18} cm^{-3}, this result is quite consistent with the extracted result by TFE model. To sum up, the effect of carbon ion implantation is not adjusting the SBH but simply increasing the carrier concentration.

4-2 Low Barrier Height Extractions

So far, the work for ensuring the feasibility of the extraction procedure is complete, and following are the studies toward the goal of low SBH extraction. In order to engage with the low SBH extraction, the NiGe/n-Ge Schottky junction is studied. At last, PtSi/p-Si and NiSi/p-Si Schottky junctions, the cases of the exact low SBH, are studied, including the cases with BF_2^+ ion implantations.

4-2 .1 Study of NiGe/n-Ge Schottky Junction

Nowadays, Si based MOSFETs have been successfully scaled down to 20 nm regime, but the continued scaling will suffer from several physical and technical limitations. With high carrier mobility and better process compatibility, Ge is considered as a potential candidate for high mobility-channel material in next generation. However, there is severe Fermi-level pinning effect in the metal/n-Ge Schottky junction resulting in high contact resistance, and here shows NiGe/n-Ge Schottky junction for example.

The electrical characteristics and extracted results are shown in Fig.4-5. The extracted results by the TE model and the TFE model are not consistent. The ideality factor shows that the conducting mechanism is not TE, and the J-V curve shows no linear region in the voltage range of measurement. It means that the defect density in Ge substrate is too high, so the conducting mechanism at forward bias is not

dominated by Schottky barrier but by the defects. However, the current at reverse bias seems to be saturated when applied voltage is larger, and it means the conducting mechanism at reverse bias is still dominated by TFE, so the extraction result from TFE model is more conceivable.

4-2 .2 PtSi/ and NiSi/p-Si Schottky Junction

In this sub-section, the cases with the lowest SBH in this thesis are studied. According to the literature, PtSi/p-Si and NiSi/p-Si SBHs are about 0.25 and 0.45 eV, respectively [17]. NiSi/p-Si Schottky junction could be regarded as a transitive case and PtSi/p-Si is the exact low SBH needed to be studied in this section.

The cases of both two junctions without BF_2^+ ion implantation are studied at first. The electrical characteristics are shown in Figs.4-6 and 4-7, and the extracted results are listed in Tables 4-1 to 4-4. For the PtSi/p-Si sample, the extracted BH0s are not consistent at different temperature, and the value of BH0 seems to be smaller as the temperature decreases. The reason why the extractions here do not work well is due to the fact that the temperature control of the low temperature probe station is not precise enough. However, the results of the TE and the TFE models are consistent, and the SBH is consistent with that reported in the literature: the SBH is about 0.25 eV when the measurement temperature is over 200 K, and the SBH is lowered down below 200 K [29]. There may be other physical reasons why the BH0 lowered down as the measurement temperature decreasing, and more details will be discussed in Section 4.3.

For the case of NiSi/p-Si, the extracted results by the TE and the TFE models are also consistent with those reported in literature, and the effect that the SBH lowers down as the temperature decreases can be observed here. For the NiSi/p-Si and

NiSi/n-Si samples, the SBHs without IFBL model at the temperature of 300 K are about 0.45 and 0.65 eV. The summation of these two SBHs is equal to the band gap of Si, and it means that the distribution of the interface states for the same metal contact is similar in either p- or n-type semiconductor.

4-2 .3 Effect of BF_2^+ Ion Implantation

The study on the PtSi/p-Si and NiSi/p-Si Schottky contacts shows that the extraction procedure is powerful and reliable even in the cases of low SBHs. However, the case of low SBH with ion implantation is not studied yet, and following are the cases of ion implantation. The implantation energy was set to 30 keV, and the doses were 1×10^{12}, 6×10^{12}, and 3×10^{13} cm^{-2}. The projected range at the implantation energy is about 24 nm, and the exact junction depth is shallower than the simulation setting due to the Si consumption during the silicide formation.

The cases of PtSi/ and NiSi/p-Si with BF_2^+ ion implantation at a dose to 1×10^{12} cm^{-2} are studied first. The electrical characteristics are shown in Figs.4-8 and 4-9. The results extracted by the TE model are not shown here, because the extracted ideality factors are all larger than 2 so that the extracted p^+/p SBHs are meaningless. The results extracted by TFE model are listed in Tables 4-5 and 4-6. After this ion implantation, the extracted BH0s of PtSi/p-Si junction were raised to 0.27 eV, but those of NiSi/p-Si junction were lowered to 0.4 eV.

At last, the cases with BF_2^+ ion implantation to higher doses are not be discussed in numerical analysis because the conducting mechanism at reverse bias is not dominated by the TFE model anymore, and the extracted effective results by the TE model are meaningless. However, the electrical characteristics with BF_2^+ ion implantation to higher doses are still shown from Fig.4-10(a) to (d). The temperature

dependence of the leakage current and the rectifying effect become weaker for both PtSi and NiSi/p-Si Schottky junctions with BF_2^+ ion implantation to a dose of 6×10^{12} cm^{-2}. When the dose rises to 3×10^{13} cm^{-2}, the rectifying effect disappears completely even at the temperature of 100 K. In other words, the SBH is lowered down effectively due to the BF_2^+ ion implantation to high doses.

4-3 Temperature Dependence

The temperature dependence of the SBH has been mentioned in Section 4-1, and both the Ni/n-SiC and NiSi/n-Si junctions showed the temperature dependence of the SBH. However, the temperature dependence of the SBH is due to the IFBL effect, and the extracted SBHs without IFBL effect at different temperature are the same. Such issue has been discussed before, but most of the literatures extracted the SBH with considering the IFBL effect [57-60]. In other words, the temperature dependence of the SBH without considering the IFBL effect, the "true" temperature dependent SBH, is still unclear. By utilizing the extraction procedure with the TFE model in Section 4-2.2, we observed the temperature dependence of the SBH without considering the IFBL effect in the low temperature measurement, and following were the details. This section only discussed the PtSi/p-Si and NiSi/p-Si Schottky junctions and those with the BF_2^+ ion implantation to a dose of 1×10^{12} cm^{-2}, and the extracted results are shown in Fig.4-11.

The cases without BF_2^+ ion implantation are discussed at first. For PtSi/p-Si, the possible reason why the BH0s lowered down from 0.25 to 0.17 eV as the temperature decreasing may be due to the lowering of the Fermi-level before the metal contacted. Fig.4-12 shows that the interface state density is high near the valence band-edge and this is consistent for most cases. As the temperature decreasing, the Fermi energy was lowered down and the Fermi-level approached to the energy level of high interface

state density, and the donor-like states above Fermi-level would be depleted. The charge neutrality level (CNL) is close to the valance band. After the high work function metal contacted, electrons transfer from semiconductor side to metal side. Because the high density of the donor-like states around the CNL, the pinning level is very close to the original CNT. Therefore, the SBH is low. The illustration is shown in Fig.4-13. The depleted donor-like states and the congregated electrons in the metal formed a dipole layer, and this dipole layer would lower down the SBH. However, the Fermi energy is higher and CNL is at the low interface state density at high temperature. After electrons transfer to metal, the pinning level is higher than that at low temperature, so is the lowering amount of the SBH. The reason why the temperature dependence of the NiSi/p-Si is not as apparent as PtSi/p-Si is because that the original pinning Fermi-level is at the energy level of low interface state density and the work function of NiSi is also low, so the charges in the dipole are only a little.

Following is the discussion of the cases with BF_2^+ ion implantation to a dose of 1×10^{12} cm^{-2}. After the ion implantation the SBH of PtSi/p-Si is increased, the possible reason is that the distribution of interface states or the crystal defects of the silicon surface layer may be differed [61-63]. However, the SBH of NiSi/p-Si junction is lowered down after the ion implantation, and we believed it would be caused by the IFBL effect due to the addition carriers in the surface by comparing the results in Section 3-2.2. The high slope region in the log(J)-V curve due to the ion implantation was not measured, so the lowering amount due to the IFBL effect could not be separated from the SBH.

4-4 Summary

The extraction procedure with the TFE model proposed in Chapter 2 is accurate from high to low SBH cases. High SBH cases of metal/SiC Schottky contacts are extracted correctly, and they are all consistent with the SBH reported in literature: the SBHs of Ni/n-SiC and Ti/n-SiC Schottky contacts are extracted as 1.42 eV and 0.85 eV. Middle SBH case of the NiSi/n-Si Schottky contact with carbon ion implantation is extracted as 0.65 eV which is also consistent with the literature. Moreover, the effect of carbon ion implantation is confirmed to act as the IFBL effect like what implanted donors act in the Schottky junction. Low SBH case of the NiGe/n-Ge Schottky contact is extracted as 0.47 eV, and the extraction with the TE model is believed to be inappropriate due to the raising of the non-ideality factor. Above all, the extraction procedure with the TFE model is also accurate for the Schottky junctions on different semiconductor materials.

For the exact low SBHs without BF_2^+ ion implantation cases, the extracted SBH of PtSi/p-Si ranges from 0.17 to 0.25 eV and the extracted SBH of NiSi/p-Si ranges from 0.42 to 0.45 eV. The exact low SBH without BF_2^+ ion implantation cases are extracted correctly with the TFE model. For the low SBHs with BF_2^+ ion implantation to a dose of 1×10^{12} cm^{-2} cases, the extracted SBHs of PtSi/p-Si are about 0.27 eV which are higher than that without BF_2^+ ion implantation by 0.02 eV, and the extracted SBHs of NiSi/p-Si ranged from 0.4 to 0.43 eV which are lower than that without BF_2^+ ion implantation. For the cases to higher doses, the dominant conducting mechanism is no long the TFE model, but the trend still can be observed: the rectifying effect is weaker as the implantation dose increases, and the Schottky junctions become purely ohmic with the BF_2^+ ion implantation to a dose of 3×10^{13} cm^{-2}.

In section 4-3, the discussion of temperature dependence explains that the lowering of the BH0 is caused from the dipole layer, and the dipole layer is formed because of the depletion of the donor-like states and the congregation of the electrons in the metal. The SBH of PtSi/p-Si junction raises after the BF_2^+ ion implantation to a dose of 1×10^{12} cm^{-2}, and it is believed that the distribution of interface states or the crystal defects of the silicon surface layer has been changed, so the SBH is pinned at different energy level. The SBH of NiSi/p-Si junction lowers down after the BF_2^+ ion implantation to a dose of 1×10^{12} cm^{-2}, and it is believed to be caused from the IFBL effect. The high slope region in the log(J)-V curve could not be measured, so the lowering amount of the IFBL effect could not be separated from the BH0.

Table 4-1 Traditional TE extraction results of PtSi/p-Si Schottky junction without BF_2^+ ion implantation.

TE	100 K	125 K	150 K	175 K	200 K	225 K
BH (eV)	0.161	0.188	0.203	0.239	NA	NA
N	1.96	2.12	1.14	~1	NA	NA

Table 4-2 TFE extraction results of PtSi/p-Si Schottky junction without BF_2^+ ion implantation.

TFE	100 K	125 K	150 K	175 K	200 K	225 K
BH0 (eV)	0.171	0.191	0.200	0.232	0.245	0.246
BH (eV)	0.161	0.181	0.191	0.221	0.233	0.232
N (cm^{-3})	1.77×10^{15}	1.89×10^{15}	1.88×10^{15}	3.29×10^{15}	4.18×10^{15}	4.59×10^{15}

Table 4-3 Traditional TE extraction results of NiSi/p-Si Schottky junction without BF_2^+ ion implantation.

TE	125 K	150 K	175 K	200 K
BH (eV)	0.390	0.408	0.406	0.421
n	~1	1.07	1.01	1.02

TE	225 K	250 K	275 K	300 K
BH (eV)	0.424	0.437	0.436	0.448
n	~1	~1	1.02	1.11

Table 4-4 TFE extraction results of NiSi/p-Si Schottky junction without BF_2^+ ion implantation.

TFE	125 K	150 K	175 K	200 K
BH0 (eV)	N.A.	0.426	0.425	0.423
BH (eV)	N.A.	0.404	0.410	0.411
N (cm^{-3})	N.A.	6.29×10^{15}	4.09×10^{15}	1.88×10^{15}

TFE	225 K	250 K	275 K	300 K
BH0 (eV)	0.433	0.447	0.441	0.449
BH (eV)	0.419	0.432	0.427	0.435
N (cm^{-3})	2.66×10^{15}	3.83×10^{15}	3.11×10^{15}	3.37×10^{15}

Table 4-5 TFE extraction results of PtSi/p-Si Schottky junction with BF_2^+ ion implantation at a dose of 1×10^{12} cm^{-2}.

TFE	175 K	200 K	225 K	250 K
BH0 (eV)	0.263	0.269	0.263	0.268
BH (eV)	0.249	0.256	0.252	0.258
N (cm^{-3})	6.64×10^{15}	5.22×10^{15}	3.83×10^{15}	3.27×10^{15}

Table 4-6 TFE extraction results of NiSi/p-Si Schottky junction with BF_2^+ ion implantation at a dose of 1×10^{12} cm^{-2}.

TFE	225 K	250 K	300 K
BH0 (eV)	0.404	0.415	0.425
BH (eV)	0.387	0.399	0.415
N (cm^{-3})	6.31×10^{15}	5.93×10^{15}	1.61×10^{15}

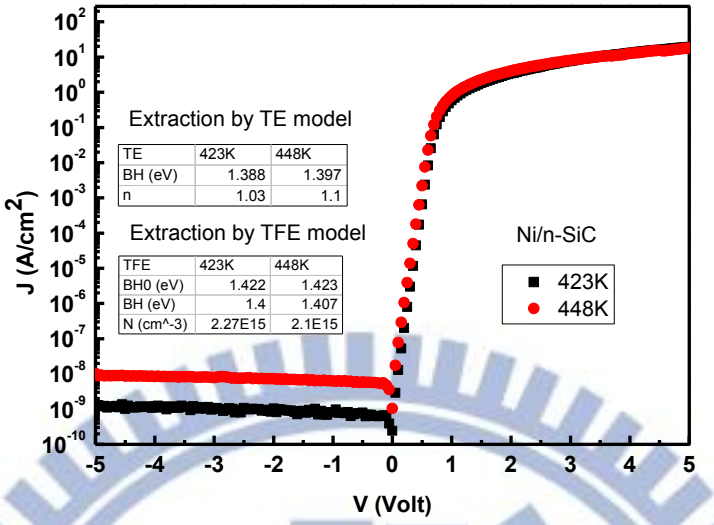

Fig.4-1 Electrical characteristics of Ni/n-SiC Schottky junction are measured at temperature of 423 and 448 K, including the extraction results by both TE and TFE model.

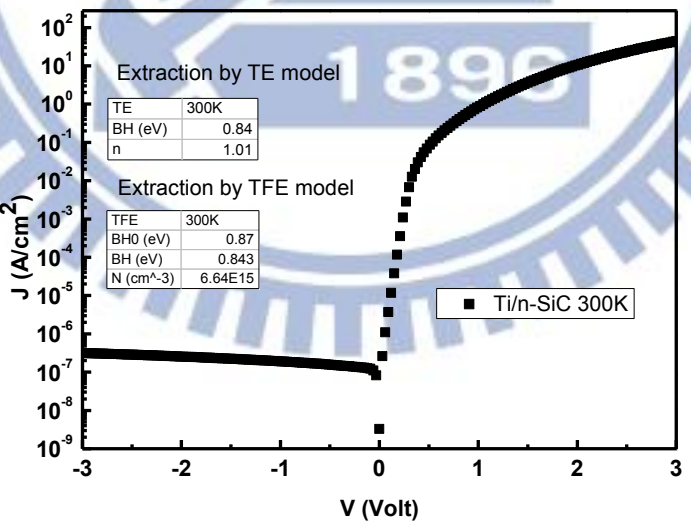

Fig.4-2 Electrical characteristics of Ti/n-SiC Schottky junction are measured at temperature of 300 K, including the extraction results by both TE and TFE model.

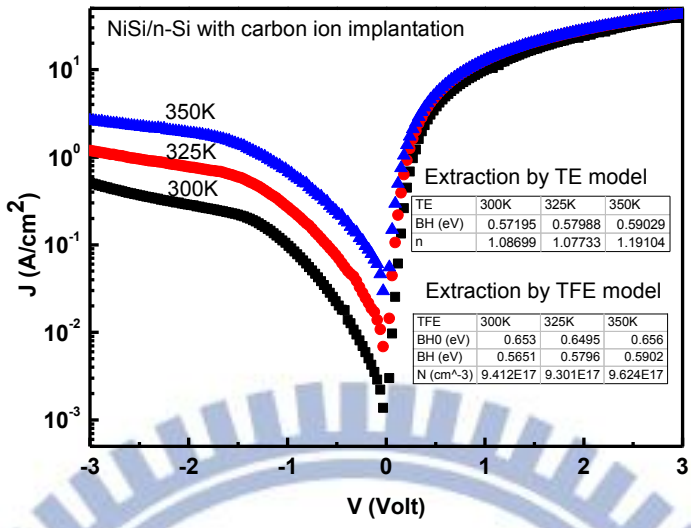

Fig.4-3 Electrical characteristics of NiSi/n-Si Schottky junction with carbon ion implantation are measured at temperature of 300, 325, and 325 K, including the extraction results by both TE and TFE model.

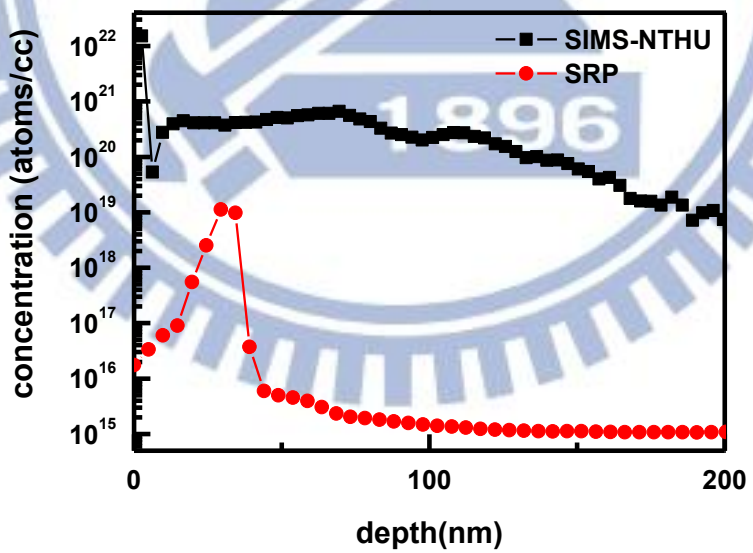

Fig.4-4 SIMS measurement before silicide formation shows the high concentration of carbon ion near the Schottky junction. SRP measurement shows that the carrier concentration near the junction is only about 10^{18} cm^{-3}.

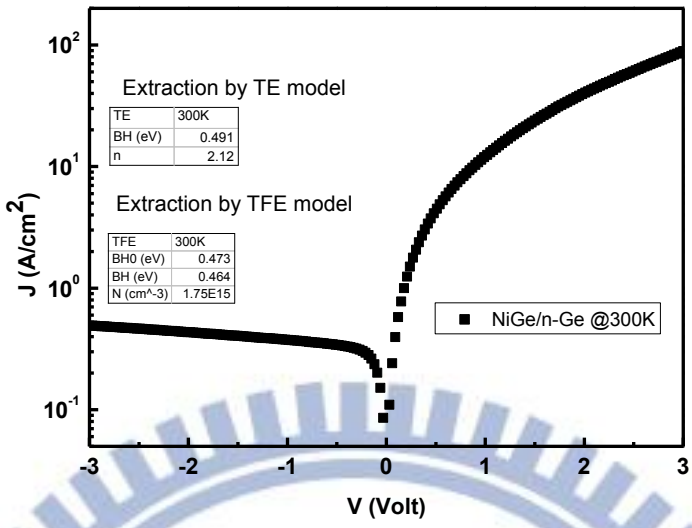

Fig.4-5 Electrical characteristics of NiGe/n-Ge Schottky junction are measured at temperature of 300 K, including the extraction results by both TE and TFE model.

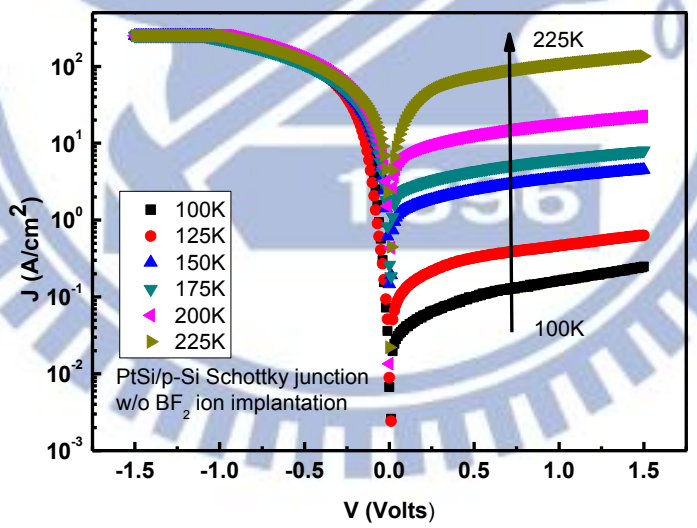

Fig.4-6 Electrical characteristics of PtSi/p-Si Schottky junction without ion implantation are measured at the temperature from 100 to 225 K.

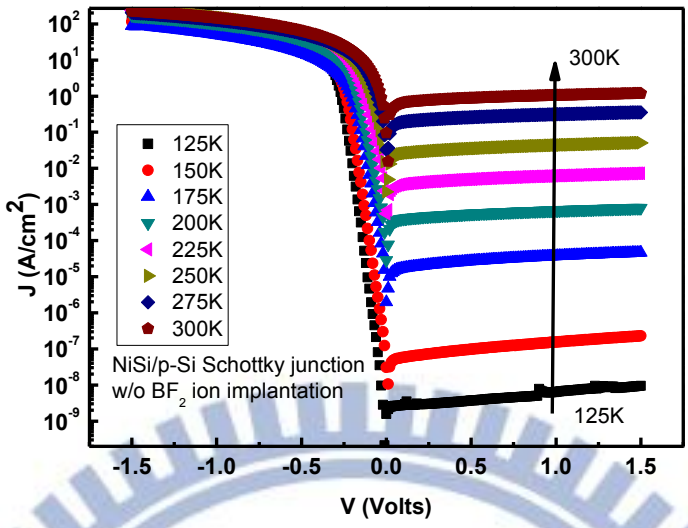

Fig.4-7 Electrical characteristics of NiSi/p-Si Schottky junction without ion implantation are measured at the temperature from 125 to 300 K.

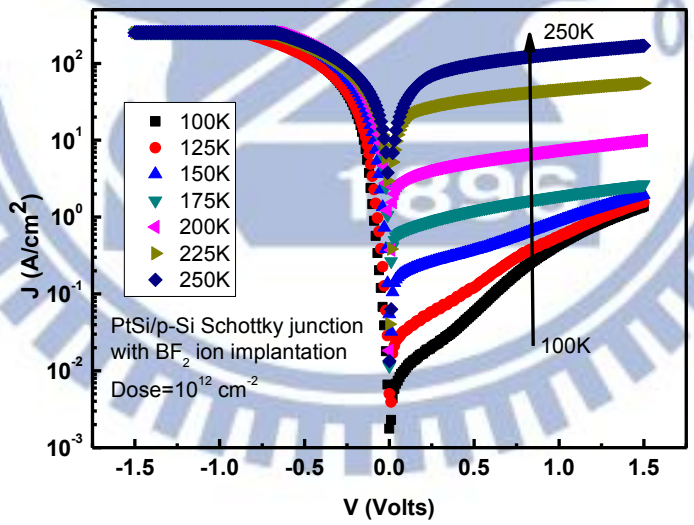

Fig.4-8 Electrical characteristics of PtSi/p-Si Schottky junction with BF_2^+ ion implantation at a dose of 1×10^{12} cm^{-2} are measured at the temperature from 100 to 225 K.

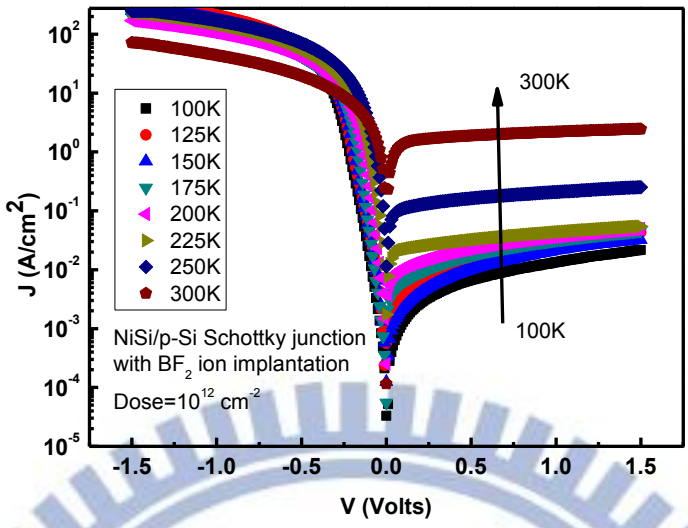

Fig.4-9 Electrical characteristics of NiSi/p-Si Schottky junction with BF_2^+ ion implantation at a dose of 1×10^{12} cm^{-2} are measured at the temperature from 100 to 300 K.

(a)

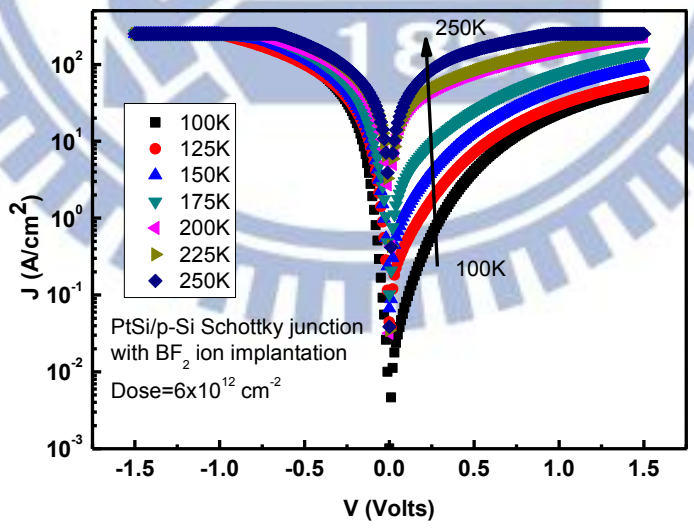

(b)

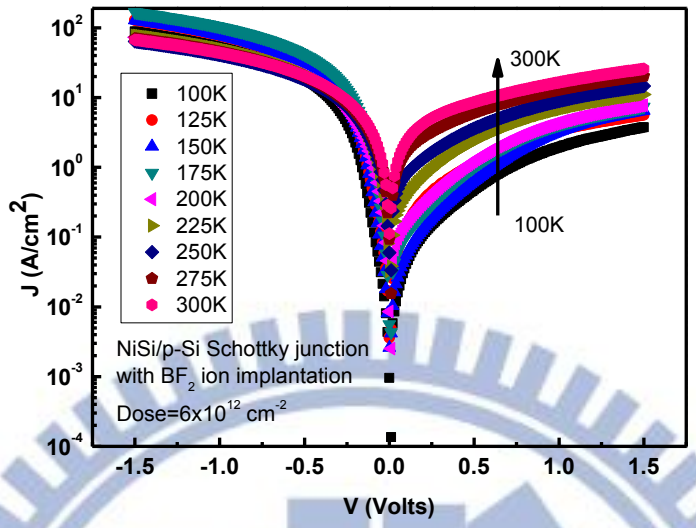
300K
100K
100K
125K
150K
175K
200K
225K
250K
275K
300K
NiSi/p-Si Schottky junction
with BF2 ion implantation
Dose=6x10^12 cm^-2
J (A/cm^2)
V (Volts)

(c)

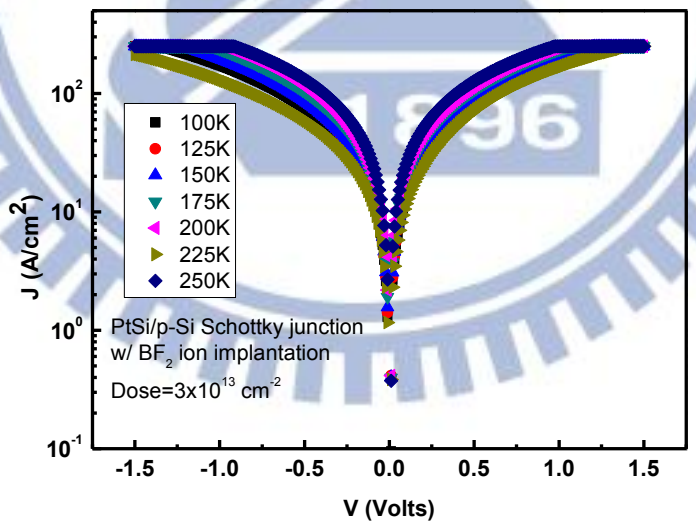
100K
125K
150K
175K
200K
225K
250K
PtSi/p-Si Schottky junction
w/ BF2 ion implantation
Dose=3x10^13 cm^-2
J (A/cm^2)
V (Volts)

(d)

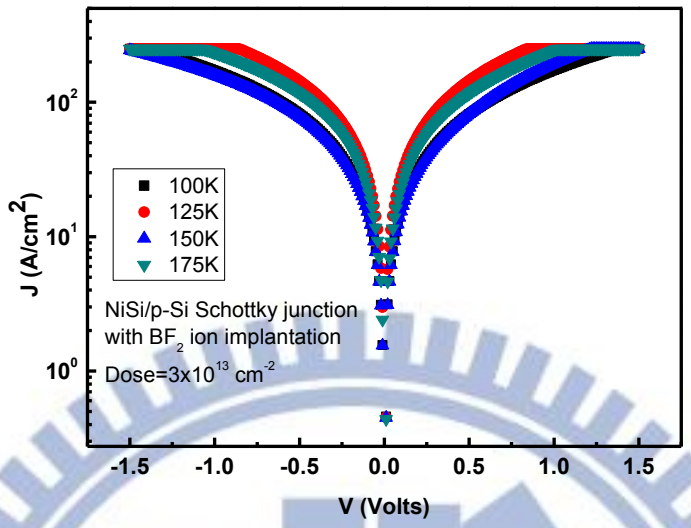

Fig.4-10 Electrical characteristics of Metal/p-Si Schottky junction with BF2+ ion implantation at a dose of 6×10^{12} cm^{-2} are measured at the temperature from 100 to 300 K (a) PtSi/p-Si: implantation is at a dose 6×10^{12} cm^{-2} (b) NiSi/p-Si: implantation is at a dose 6×10^{12} cm^{-2} (c) PtSi/p-Si: implantation is at a dose 3×10^{13} cm^{-2} (d) NiSi/p-Si: implantation is at a dose 3×10^{13} cm^{-2}

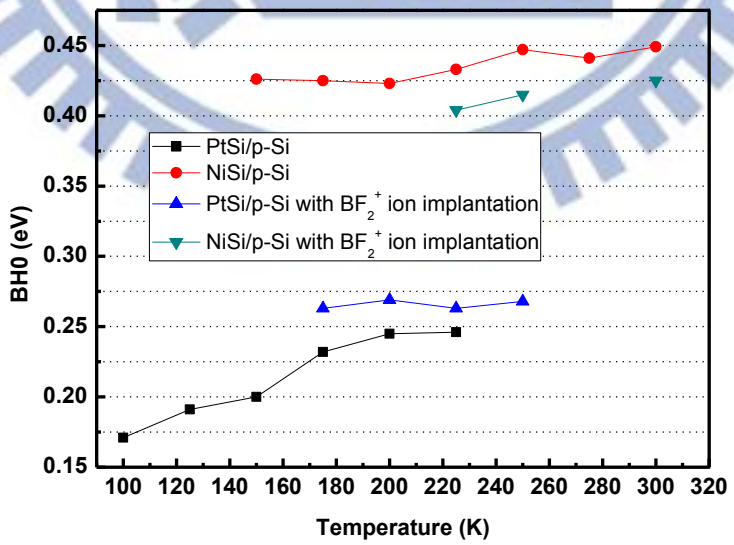

Fig.4-11 The temperature dependence of the BH0 without considering the IFBL effect.

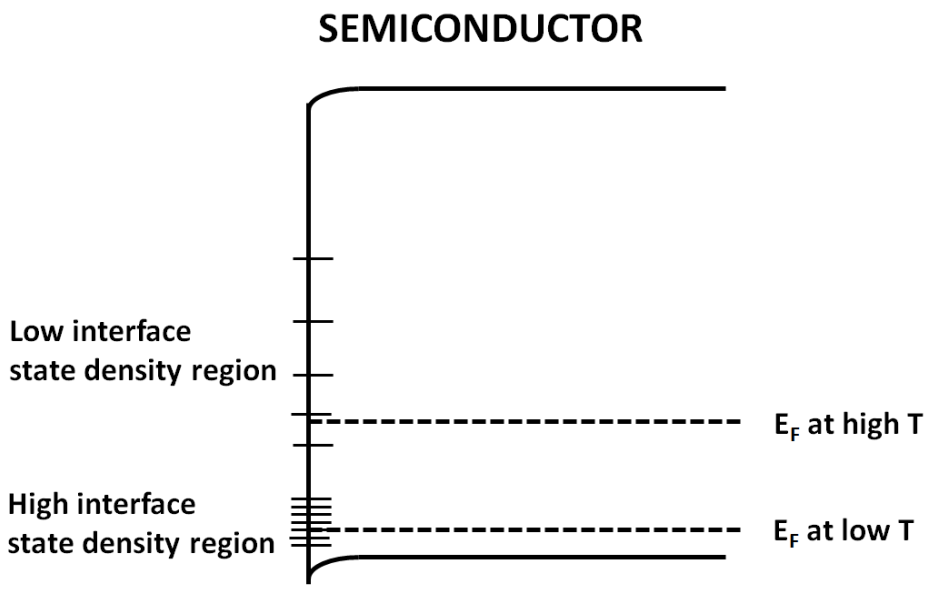

Fig.4-12 Illustration of the Fermi energy level and the donor-like interface state density before metal contact.

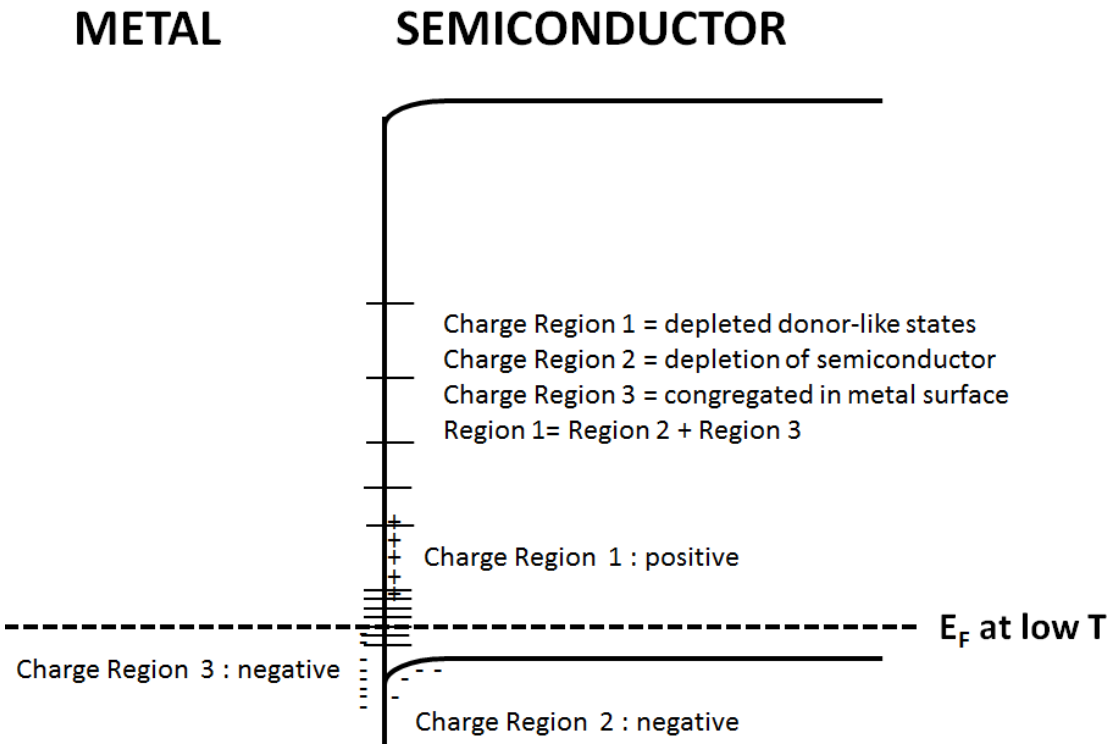

Fig.4-13 Illustration of the charge distribution in the Schottky junction.

Chapter 5

Conclusions and Future Works

5-1 Conclusions

In this thesis, the extraction procedure for Schottky barrier height with the TFE model is studied. First, the procedure is verified by the TCAD simulation including the Schottky junctions with constant doping profiles and Gaussian doping profiles. We found out that the IFBL model in the TCAD simulation does not fit the real cases due to the simplification of the simulation tool. In the case of SBH = 0.3 eV with a constant doping profile, the temperature limits of the TE model and the TFE model are commented: the feasible extracting temperature of the TFE model is promoted by 100 K. As SBH = 0.3 eV with a Gaussian doping profile, the effect of the non-uniformly doped region on the SBH extractions commented: first, the deeper junction depth cases showed that the IFBL effect can be observed in the I-V characteristic at reverse bias, and the TFE model is capable of separating the lowering amount of SBH due to the IFBL effect. Second, the case of shallower junction depth and lower peak concentration shows that the IFBL effect disappeared in the I-V characteristic at reverse bias due to the fully depletion of the non-uniformly doped region at zero bias, and the lowering amount of SBH due to the IFBL effect is insignificant. In this case, the extracted SBH would be the value including the IFBL effect but not the true physical barrier height. In the case of shallow junction depth but high peak concentration, the simulation shows that the rectifying effect disappears even at low temperature so that the SBH can be extracted by neither TFE nor TE model.

After the verification by simulation works, the extraction procedure is applied to

the real Schottky junctions. For the metal/SiC Schottky junction cases, the results show that the extraction by either the TE model or the TFE model exhibits a good accuracy for high SBH cases. For the NiSi/n-Si Schottky junction with carbon ion implantation case, the result shows that the TE model is not appropriate to extract the SBH due to the fact that the lowering amount of the SBH due to the IFBL effect could not be extracted. However, the TFE model can determine the lowering amount of the SBH, and the SBH without the IFBL effect is extracted as the origin NiSi/n-Si Schottky junction. The activated carbon ions are believed to contribute extra carriers for n-type semiconductor, so the IFBL effect is more apparent due to the high doped region near the surface. For the NiGe/n-Ge Schottky junction, the extraction by the TE model at room temperature is believed to be inappropriate due to the raising of the ideality factor. The medium SBHs from 0.45 to 0.65 eV can be extracted accurately and the effect of the fabrication process can be clarified by the extraction procedure with the TFE model.

The low SBH extraction performed on the PtSi/p-Si Schottky junction shows strong temperature dependence of the SBH. In low temperature region, the donor-like interface states are depleted abundantly and induce much of electrons. After the metal contacted, the excessive electrons which cannot be stayed in the semiconductor will be transferred to the metal, which is a low potential material in comparison. The electrons congregated in the metal and the depleted donor-like states will form a dipole layer, and the SBH is effectively lowered down due to this layer. However, the depleted donor-like states are only a bit in high temperature region, so the electrons accumulated in the metal decrease. The effect of the dipole layer becomes unapparent, and the SBH is not lowered down obviously. The BF_2^+ ion implantation on the NiSi/p-Si Schottky junction shows that the extracted SBH is effectively lowered down like what simulation works: the IFBL effect affects the extracted SBH but cannot be

identified individually. The I-V characteristics of the PtSi/p-Si and NiSi/p-Si Schottky junctions with BF_2^+ ion implantation at 30 KeV to a dose of $3\times10^{13}\,cm^{-2}$ or higher are determined by the parasitic resistance even at low temperature, and the SBH can be extracted by neither the TE nor the TFE model.

Above all, this thesis proposed an efficient and accurate procedure for the SBH extraction. The extraction procedure proposed in Chapter 2 exhibits a good performance from high to low SBH cases and from wide to narrow band gap semiconductor materials. The operation is simple and the computing time is short. Utilizing the I-V characteristic at reverse bias, the feasible extracting temperature is improved. Considering the field emission, the extraction with the TFE model is more reliable than that with the TE model. The only one demerit is that the procedure loses the capability to determine the IFBL effect in Schottky junctions with shallow and non-uniformly doped surface layer.

5-2 Future Works

The extraction procedure proposed in Chapter 2 still could be improved: the algorithm of computing could be more efficiency and the bounding value for extracting could be removed from the program. More conducting mechanisms should be considered to make the procedure more powerful, e.g. the trap-assisted tunneling through the SBH and the generation current are dominant mechanism in the high defect concentration case. The conducting mechanism of the Schottky junctions with BF_2^+ ion implantation below some specific temperature is still unknown, and it should be investigated further. The low temperature measurement was not done well in this study, and it should be performed with a more precise temperature control. The junction depth of the BF_2^+ ion implantation is too shallow, and the effects of boron

and fluorine ions cannot be discussed individually. The ion implantation could be performed by B^+ ions, and the junction depth would be deeper such that the IFBL effect could be identified. Furthermore, the exact low SBH cases of the metal/n-Si Schottky junctions have not been studied yet. In order to observe the changing of the interface states near the conduction band edge at low temperature, low SBH cases of metal/n-Si Schottky junctions should be investigated further. In order to discuss the inhomogeneity of the SBH, more material analysis, e.g. TEM, SEM and SIMS, could be investigated to make up the insufficiency of this study.

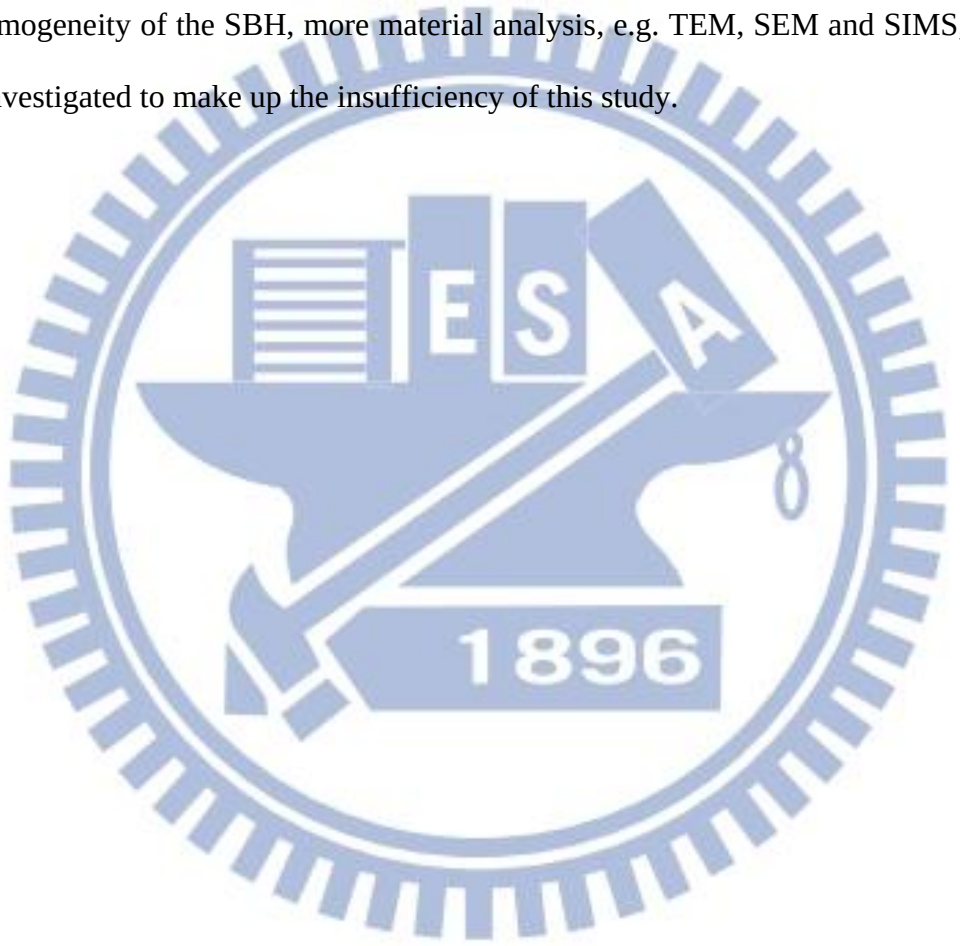

References

[1]. F. Braun, “Uber die Stromleitung durch Schwefelmetalle,” *Ann. Phys.*, vol. 229, no. 12, pp. 556–563, 1874.

[2]. H. C. Torrey and C. A. Whitmer, *Crystal Rectifiers*, New York: McGraw-Hill, 1948.

[3]. W. Schottky, R. Stromer, and F. Waibel, *Hochfrequenztechnik*, vol. 37, pp. 162–165, 1931

[4]. H. A. Bethe, “Theory of the boundary layer of crystal rectifiers,” *MIT Radiation Laboratory report*, no. 43/12, 1942.

[5]. B. L. Sharma, *Metal-Semiconductor Schottky Barrier Junctions and Their Applications*, New York: Plenum Press, pp. 2–8, 1984.

[6]. J. Bardeen, “Surface states and rectification at a metal-semiconductor contact,” *Phys. Rev.*, vol. 71, pp. 717–727, 1947.

[7]. B. L. Sharma, *Metal-Semiconductor Schottky Barrier Junctions and Their Applications*, New York: Plenum Press, p. 9, 1984.

[8]. J. Robertson and L. Lin, “Fermi Level pinning in Si, Ge and GaAs systems – MIGS or defects?,” *in IEDM Tech. Dig.*, 2009, pp. 119–122.

[9]. W. Monch, “Barrier heights of real Schottky contacts explained by metal-induced gap states and lateral inhomogeneities,” *J. Vac. Sci. Technol. B*, vol. 17, no. 4, pp. 1867–1876, 1999.

[10]. H. Hasegawa and H. Ohno, “Unified disorder induced gap state model for insulator–semiconductor and metal–semiconductor interfaces,” *J. Vac. Sci. Technol. B*, vol. 4, no. 4, pp. 1130–1138, 1986.

[11]. J. Tersoff, “Schottky Barrier Heights and the Continuum of Gap States,” *Phys. Rev. Lett.*, vol. 52, no. 6, pp. 465–468, 1984.

[12]. M. Y. Ali and M. Tao, “Effect of Sulfur Passivation of Silicon (100) on Schottky Barrier height: Surface States versus Surface Dipoles,” *J. Appl. Phys.*, vol. 101, no. 10, pp. 103708–103708-5, 2007

[13]. S. M. Sze and K. K. Ng, *Physics of semiconductor Devices*, New York: Wiley, p. 250, 1981.

[14]. E. Dubois and G. Larrieu, “Low Schottky barrier source/drain for advanced MOS architecture: device design and material consideration,” *Solid-State Electron.*, vol. 46, no. 7, pp. 997–1004, 2002.

[15]. D. Connelly, C. Faulkner, and D. E. Grupp, “Performance advantage of Schottky source/ drain in ultrathin-body silicon-on-insulator and dual-gate CMOS,” *IEEE Trans. Electron Dev.*, vol. 50, no. 5, pp. 1340–1345, 2003.

[16]. D. Connelly, C. Faulkner, and D. E. Grupp, “Optimizing Schottky S/D offset for 25 nm dual-gate CMOS performance,” *IEEE Electron Device Lett.*, vol. 24, no. 6, pp. 411–413, 2003.

[17]. S. M. Sze and K. K. Ng, *Physics of semiconductor Devices*, New York: Wiley, pp. 279–293, 1981.

[18]. S. P. Murarka, “*Silicides for VLSI Applications*,” Academic Press, New York, 1983.

[19]. A. Kikuchi, “Correlation between Schottky barrier height and the heat of formation of transition- metal silicides,” *J. Appl. Phys.*, vol. 74, no. 5, pp. 3270–3272, 1993.

[20]. O. Nur, M. Willander, R. Turan, M. R. Sardela, and G. V. Hansson, “Metal-semiconductor junctions on p-type strained $Si_{1-x}Ge_x$ layers,” *Appl. Phys.*

Lett., vol. 68, no. 8, pp. 1084–1086, 1996.

[21]. C. R. Crowell, "The Richardson Constant for Thermionic Emission in Schottky Barrier Diodes," *Solid-State Electron.*, vol. 8, no. 4, pp. 395–399, 1965.

[22]. C. R. Crowell and S. M. Sze, "Current Transport in Metal-Semiconductor Barriers," *Solid-State Electron.*, vol. 9, no. 11–12, pp. 1035–1048, 1966.

[23]. A. M. Goodman, "Metal-Semiconductor Barrier Height Measurement by Differential Capacitance-Method –One Carrier System," *J. Appl. Phys.*, vol. 34, no. 2, pp. 329–338, 1963

[24]. J. M. Shannon, "Reducing the effective height of a Schottky barrier using low-energy ion implantation," *Appl. Phys. Lett.*, vol. 24, no. 8, pp. 369–371, 1974

[25]. J. M. Shannon, "Increasing the effective height of a Schottky barrier using low-energy ion implantation," *Appl. Phys. Lett.*, vol. 25, no. 1, pp. 75–77, 1974

[26]. J. L. Freeouf, T. N. Jackson, S. E. Laux, and J. M. Woodall, "Size dependence of effective barrier heights of contacts," *J. Vac. Sci. Technol.*, vol. 21, no. 2, pp. 570–573, 1982.

[27]. R. F. Schmitsdorf, T. U. Kampen, and W. Mönch, "Explanation of the linear correlation between the barrier heights and ideality factors of real metal-semiconductor contacts by laterally nonuniform Schottky barriers," *J. Vac. Sci. Technol.*, vol. 15, no. 4, pp. 1221–1226, 1997.

[28]. H. S. Wong, L. Chan, G. Samudra, and Y. C. Yeo, "Effective Schottky barrier height reduction using sulfur or selenium at the NiSi/Si(100) interface for low resistance contact," *IEEE Electron Device Lett.*, vol. 28, no. 12, pp. 1102–1104, 2007.

[29]. E. Dubois and G. Larrieu, “Measurement of low Schottky barrier heights applied to metallic source/drain metal–oxide–semiconductor field effect transistors,” *J. Appl. Phys.*, vol. 96, no. 1, pp. 729–737, 2004.

[30]. C. R. Crowell and V. L. Rideout, “Normalized thermionic-field (TF) emission in metal-semiconductor (Schottky) barriers,” *Solid-State Electron.*, vol. 12, no. 2, pp. 89–105, 1969.

[31]. Synopsys Sentaurus TCAD software.

[32]. K. J. Schoen, J. P, Henning, J.M. Woodall, Jr. J. A. Cooper, and M. R. Melloch, “A dual-metal-trench (DMT) Schottky pinch-rectifier in 4H-SiC,” *IEEE Electron Device Lett.*, vol. 19, no. 4, pp. 97–99, 1998.

[33]. V. Khemka, V. Ananthan, and T. P. Chow, “A fully planarized 4H-SiC trench MOS barrier Schottky (TMBS) rectifier,” *IEEE Electron Device Lett.*, vol. 21, no. 6, pp. 286–288, 2000.

[34]. F. Roccaforte, F. La Via, A. La Magna, S. Di Franco, and S. Raineri, “Silicon carbide pinch rectifiers using a dual-metal Ti-Ni/sub 2/Si Schottky barrier,” *IEEE Trans. Electron Devices*, vol. 50, no. 8, pp. 1741–1747, 2003.

[35]. B. J. Skromme, E. L. Luckowski, K. Moore, M. Bhatnagar, C. E. Weitzel, T. Gehoski, and D. Ganser, “Electrical characteristics of Schottky barriers on 4H–SiC: the effects of barrier height nonuniformity,” *J. Electron. Mater.*, vol. 29, no. 3, pp. 376–383, 2000.

[36]. X. Ma, P. Sadagopan, and T. S. Sudarshan, “Investigation on barrier inhomogeneities in 4H-SiC Schottky rectifiers,” *physica status solidi (a)*, vol. 203, no. 3, pp. 643–650, 2006.

[37]. D. J. Ewing, Q. Wahab, R. R. Ciechonski, M. Syväjärvi, R. Yakimova, and L. M. Porter, “Inhomogeneous electrical characteristics in 4H-SiC Schottky diodes,” *Semiconductor Science and Technology*, vol. 22, no. 12, pp. 1287–

1291, 2007.

[38]. M. E. Aydın, N. Yıldırım, and A. Turut "Temperature-dependent behavior of Ni/4H-nSiC Schottky contacts," *J. Appl. Phys.*, vol. 102, no. 4, pp. 043701-1–043701-7, 2007.

[39]. Z. J. Qiu, Z. Zhang, M. Ö stling, and S. L. Zhang, "A comparative study of two different schemes to dopant segregation at NiSi/Si and PtSi/Si interfaces for Schottky barrier height lowering," *IEEE Trans. Electron Devices*, vol. 55, no. 1, pp. 396–403, 2008.

[40]. J. M. Andrews and F. B. Koch, "Formation of NiSi and current transport across the NiSi-Si interface," *Solid-State Electron.*, vol. 14, no. 10, pp. 901–908, 1971

[41]. D. J. Coe and E. H. Rhoderick, "Silicide formation in Ni-Si Schottky barrier diodes," *J. Phys. D*, vol. 9, no. 6, pp. 965–972, 1976.

[42]. J. Chan , N. Y. Martinez , J. J. D. Fitzgerald , A. V. Walker , R. A. Chapman , D. Riley , A. Jain , C. L. Hinkle, and E. M. Vogel, "Extraction of correct Schottky barrier height of sulfur implanted NiSi/n-Si junctions: Junction doping rather than barrier height lowering," *Appl. Phys. Lett.*, vol. 99, no. 1, pp. 012114–012114-3, 2011.

[43]. B. Y. Tsui and C. M. Lee, "Thermal stability of nickel silicide and shallow junction electrical characteristics with carbon ion implantation," *Japanese Journal of Applied Physics*, vol. 49, no. 4, pp. 04DA04–04DA04-6, 2010.

[44]. I. Ban, M. C. Ozturk, and E. K. Demirlioglu, "Suppression of oxidation-enhanced boron diffusion in silicon by carbon implantation and characterization of MOSFETs with carbon-implanted channels," *IEEE Trans. Electron Devices*, vol. 44, no. 9, pp. 1544–1551, 1997.

[45]. A. Dimoulas, P. Tsipas, A. Sotiropoulos and E. K. Evangelou, "Fermi level pinning and charge neutrality level in germanium," *Appl. Phys. Lett.*, vol. 89, no.

25, pp. 252110–252110-3, 2006.

[46]. T. Nishimura, K. Kita and A. Toriumi, “Evidence for strong Fermilevel pinning due to metal-induced gap states at metal/germanium interface,” *Appl. Phys. Lett.*, vol. 91, no. 12, pp. 123123–123123-3, 2007.

[47]. V. W. L. Chin, J. W. V. Storey, and M. A. Green, “Characteristics of p-type PtSi Schottky diodes under reverse bias,” *J. Appl. Phys.*, vol. 68, no. 8, pp. 4127–4132, 1990.

[48]. A. Kikuchi, “Correlation between Schottky-barrier height and the heat of formation of transition-metal silicides,” *J. Appl. Phys.*, vol. 74, no. 5, pp. 3270–3272, 1993.

[49]. O. Nur, M. Willander, R. Turan, M. R. Sardela, and G. V. Hansson, “Metal–semiconductor junctions on p-type strained Si_{1-x} Ge_x layers,” *Appl. Phys. Lett.*, vol. 68, no. 8, pp. 1084–1086, 1996.

[50]. V. W. L. Chin, J. W. V. Storey, and M. A. Green, “Characteristics of p-type PtSi Schottky diodes under reverse bias,” *J. Appl. Phys.*, vol. 68, no. 8, pp. 4127–4132, 1990.

[51]. C. Y. Chang and S. M. Sze, “Carrier transport across the metal-semiconductor barriers,” *Solid State Electron.*, vol. 13, no. 6, pp. 727–740, 1970.

[52]. K. J. Schoen, J. M. Woodall, J. A. Cooper, and M. R. Melloch, “Design considerations and experimental analysis of high-voltage SiC Schottky barrier rectifiers,” *IEEE Trans. Electron. Devices*, vol. 45, no. 7, pp. 1595–1604, 1998.

[53]. F. Roccaforte, F. La Via, V. Raineri, R. Pierobon, and E. Zanoni, “Richardson’s constant in inhomogeneous silicon carbide Schottky contacts,” *J. Appl. Phys.*, vol. 93, no. 11, pp. 9137–9144, 2003.

[54]. D. Defives, O. Noblanc, C. Dua, C. Brylinski, M. Barthula, V. Aubry-Fortuna, and F. Meyer, “Barrier inhomogeneities and electrical characteristics of

Ti/4H-SiC Schottky rectifiers," *IEEE Trans. Electron Devices*, vol. 46, no. 3, pp. 449–455, Mar. 1999.

[55]. J. M. Larson and J. P. Snyder, "Overview and status of metal S/D Schottky-barrier MOSFET technology," *IEEE Trans. Electron. Devices*, vol. 53, no. 5, pp. 1048–1058, 2006.

[56]. J. Luo, Z. Qiu, D. W. Zhang, P. E. Hellström, M. Ö stling, and S. L. Zhang, "Effects of carbon on effective Schottky barrier heights of NiSi modified by means of dopant segregation," *IEEE Electron Device Lett.*, vol. 30, no. 6, pp. 608–610, 2009.

[57]. J. H. Werner and H. H. Gutler, "Temperature dependence of Schottky barrier heights on silicon," *J. Appl. Phys.*, vol. 73, no. 3, pp. 1315–1320, 1993.

[58]. A. M. Crowley and S. M. Sze, "Surface States and Barrier Heights of Metal-Semiconductor Systems," *J. Appl. Phys.*, vol. 36, no. 10, pp. 3212–3220, 1965.

[59]. M. O. Aboelfotoh, "Temperature dependence of the Schottky-barrierheight of tungsten on n-type and p-type silicon," *Solid-State Electron.*, vol. 34, no. 1, pp. 51–55, 1991.

[60]. S. Chand, J. Kumar, "Effects of barrier height distribution on the behavior of a Schottky diode," *J. Appl. Phys.*, vol. 82, no. 10, pp. 5005–5010, 1997.

[61]. B. Y. Tsui, J. Y. Tsai, T. S. Wu, and M. C. Chen, "Effect of fluorine incorporation on the thermal stability of PtSi/Si structure," *IEEE Trans. Electron Devices*, vol. 40, no. 1, pp. 54–63, 1993.

[62]. D. N. Kouvatsos, F. A. Stevie, and R. J. Jaccodine, "Interface state density reduction and effect of oxidation temperature on fluorine in-corporation and profiling for fluorinated metal oxide semiconductor capacitors," *J. Electrochem. Soc.*, vol. 140, no. 4, pp. 1160–1164, 1993.

[63]. S. Ashok, H. Kräutle, and H. Beneking, “Effect of argon ion implantation dose on silicon Schottky barrier characteristics,” *Appl. Phys. Lett.*, vol. 45, no. 4, pp. 431–433, 1984.

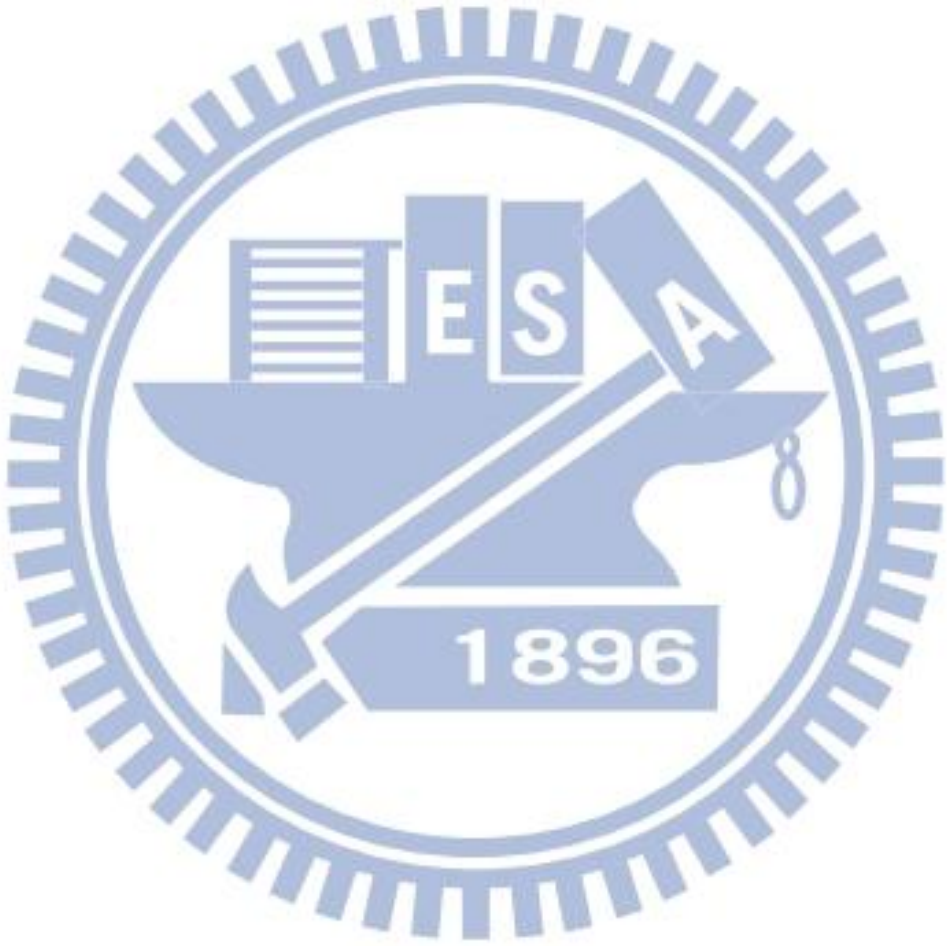

Author’s Biography

姓名：傅子瑜

性別：男

生日：民國 77 年 3 月 1 日

學歷：

高雄市立鎮昌國民小學 (83.9-87.6)

高雄縣立誠正國民小學 (87.6-89.6)

高雄縣立鳳山國民中學 (89.9-92.6)

國立鳳新高級中學 (92.9-95.6)

國立交通大學電機資訊學士班 (95.9-99.6)

國立交通大學電子研究所碩士 (99.9-101.6)

碩士論文題目：

精確且高效率之蕭基位障萃取程序

An Accurate and Efficient Procedure for Schottky Barrier Height Extraction